



Pavlidis, N., Kofinas, A., Papanikolaou, M. G., Miras, H. N., Drouza, C., Kalampounias, A. G., Kabanos, T. A., Konstandi, M. and Leondaritis, G. (2021) Synthesis, characterization and pharmacological evaluation of quinoline derivatives and their complexes with copper(II) in in vitro cell models of Alzheimer's disease. *Journal of Inorganic Biochemistry*, 217, 111393. (doi: [10.1016/j.jinorgbio.2021.111393](https://doi.org/10.1016/j.jinorgbio.2021.111393))

There may be differences between this version and the published version. You are advised to consult the publisher's version if you wish to cite from it.

<http://eprints.gla.ac.uk/234562/>

Deposited on 19 February 2021

Enlighten – Research publications by members of the University of Glasgow  
<http://eprints.gla.ac.uk>

## Title page

### Synthesis, characterization and pharmacological evaluation of quinoline derivatives and their complexes with copper(II) in *in vitro* cell models of Alzheimer's disease

#### Authors

Nikolaos Pavlidis<sup>a,b</sup>, Aristeidis Kofinas<sup>a</sup>, Michael G. Papanikolaou<sup>b</sup>, Haralampos N. Miras<sup>c</sup>, Chryssoula Drouza<sup>d</sup>, Angelos G. Kalampounias<sup>e,f</sup>, Themistoklis A. Kabanos<sup>b</sup>, Maria Konstandi<sup>a</sup>, George Leondaritis<sup>a,\*</sup>

<sup>a</sup> Department of Pharmacology, Faculty of Medicine, University of Ioannina, Ioannina 45110, Greece.

E-mail: ni\_pavlidis@yahoo.gr; ar.kofinas@gmail.com; mkonstan@uoi.gr; gleondar@uoi.gr

<sup>b</sup> Section of Inorganic and Analytical Chemistry, and <sup>e</sup> Physical Chemistry, Department of Chemistry, University of Ioannina, Ioannina 45110, Greece. E-mail: pap.mike@hotmail.com; tkampano@uoi.gr; akalamp@uoi.gr

<sup>c</sup> West CHEM, School of Chemistry, University of Glasgow, Glasgow G12 8QQ, UK. E-mail: charalampos.moiras@glasgow.ac.uk

<sup>d</sup> Department of Agricultural Sciences, Biotechnology and Food Science, Cyprus University of Technology, Limassol 3036, Cyprus. E-mail: [chryssoula.drouza@cut.ac.cy](mailto:chryssoula.drouza@cut.ac.cy)

<sup>f</sup> University Research Center of Ioannina (URCI), Institute of Materials Science and Computing, 45110, Ioannina, Greece; E-mail: akalamp@uoi.gr

#### Corresponding Author

\* George Leondaritis, Department of Pharmacology, Faculty of Medicine, University of Ioannina, Ioannina 45110, Greece; Tel: 30 26510 07555; E-mail: [gleondar@uoi.gr](mailto:gleondar@uoi.gr)

**Abbreviations:** AD, Alzheimer's disease; AChE, acetylcholinesterase; CNS, central nervous system; A $\beta$ , beta amyloid; NMDA, N-methyl-D-aspartate; APP, amyloid precursor protein; ROS, reactive oxygen species; GSK-3 $\beta$ , glycogen synthase kinase-3 beta; SOD, superoxide dismutase; H<sub>2</sub>O<sub>2</sub>, hydrogen peroxide; NMR, nuclear magnetic resonance; TLC, thin layer chromatography; DMEM, Dulbecco's Modified Eagle's Medium; CHO, Chinese hamster ovary; MTS, 3-(4,5-dimethylthiazol-2-yl)-5-(3-carboxymethoxyphenyl)-2-(4-sulfophenyl)-2H-tetrazolium, inner salt; PES, phenazine ethosulfate; HR-ESI(+)-MS, high-resolution electrospray ionization mass spectrometry; FBS, fetal bovine serum; RA, retinoic acid; EC<sub>50</sub>, half maximal effective concentration; LD<sub>50</sub>, median lethal dose; BBB, blood-brain barrier; PAS, peripheral anionic site; CAS, catalytic active site.

## ABSTRACT

Alzheimer's disease (AD) is a neurodegenerative disease of the central nervous system. The main pathophysiological mechanisms involve cholinergic neurotransmission, beta-amyloid and Tau proteins, several metal ions and oxidative stress, amongst others. Current drugs offer only relief of symptoms and not a cure of AD. Recent evidence suggests that multifunctional compounds, targeting multiple pathophysiological mechanisms, may have great potential for the treatment of AD. In this study, we report on the synthesis and physicochemical characterization of four quinoline-based metal chelators and their respective copper(II) complexes. Most compounds were non-toxic at concentrations  $\leq 5 \mu\text{M}$ . In neuroprotection studies employing undifferentiated and differentiated SH-SY5Y cells, we show that the metal chelator  $N^2, N^6$ -di(quinolin-8-yl)pyridine-2,6-dicarboxamide ( $\text{H}_2\text{dqpyca}$ ) exerts significant neuroprotection against both  $\text{A}\beta$  peptide- and  $\text{H}_2\text{O}_2$ -induced toxicities. The copper(II) complex  $[\text{Cu}^{\text{II}}(\text{H}_2\text{bqch})\text{Cl}_2] \cdot 3\text{H}_2\text{O}$  ( $\text{H}_2\text{bqch} = N, N'$ -Bis(8-quinolyl)cyclohexane-1,2-diamine) also protects against  $\text{H}_2\text{O}_2$ -induced toxicity, with an  $\text{EC}_{50}$  concentration of 80 nM. Molecular docking simulations, using the crystal structure of the acetylcholinesterase (AChE)-rivastigmine complex as a template, indicated a strong interaction of the metal chelator  $\text{H}_2\text{dqpyca}$ , followed by  $\text{H}_2\text{bqch}$ , with both the peripheral anionic site and the catalytic active site of AChE. Our findings indicate that the metal chelator  $\text{H}_2\text{dqpyca}$  and the copper(II) complex  $[\text{Cu}^{\text{II}}(\text{H}_2\text{bqch})\text{Cl}_2] \cdot 3\text{H}_2\text{O}$  appear to be worth investigating as multifunctional lead compounds for the treatment of AD.

**Keywords:** quinoline; metal complex; neuroprotection; oxidative stress; Alzheimer's disease; SH-SY5Y

## 1. Introduction

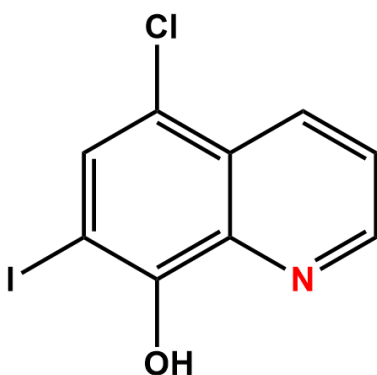
Alzheimer's disease (AD) is a neurodegenerative disease of the central nervous system, affecting mainly the elderly, and it accounts for 60-70% of dementia cases [1]. It is characterized by episodic memory loss and decline of various mental functions including cognitive ability, spatial orientation, attention and speech ability [2,3]. In recent years, AD patients have been increased dramatically due to the aging of population. As a result, AD is one of the most common diseases in our time [4,5]. In particular, according to World Health Organization, around 50 million people worldwide suffer from AD or other types of dementia [6].

AD is a multifactorial disorder, which has been attributed to exogenous and genetic factors [7,8]. Various pathophysiological mechanisms have been studied, but the main hypotheses that have primarily gained attention are those related to the cholinergic neurotransmission, the amyloid plaque deposition, Tau proteins, metal ions and oxidative stress [4,7,9–11]. The FDA-approved drugs are restricted to several acetylcholinesterase (AChE) inhibitors, such as rivastigmine, tacrine, donepezil and galantamine, which offer only symptomatic relief without curing AD [7,10,12]. Discovery of more effective compounds remains still a challenge. Currently, despite intensive research efforts, no new drugs have been developed, a fact that is mainly due to unsatisfactory results from either preclinical or clinical studies [2,12–14]. Failure of monotherapies that are based on the amyloid, metal ion and oxidative stress hypotheses has sparked interest in the development of multifunctional compounds, which are considered as the most promising for the treatment of AD, as they are related to all known hypotheses of AD [2,12–14]. In this context, metal ions, especially copper, play important roles. It should be noted that copper participates in various fundamental functions of the body, especially those related to CNS [15]. Copper is mainly bound to chaperone proteins, which reduce the amount of free copper and also help transport this metal ion into the brain [7,15]. Copper dyshomeostasis is associated with increased levels of its free toxic cation and contributes significantly to the pathophysiology of AD. One well-established mechanism for copper toxicity in AD is due to binding of free  $\text{Cu}^{\text{II}}$  to  $\text{A}\beta$

peptides, followed by increased charge, increased hydrophobicity and susceptibility to further aggregation [2,4,7]. Additional mechanisms include NMDA receptor activation which results in  $\text{Cu}^{\text{II}}$ -induced Tau phosphorylation, APP degradation and increased  $\text{A}\beta$  production [12]. Furthermore,  $\text{Cu}^{\text{II}}$  redox activity may cause oxidative stress and ROS production [5,7,16]. Apparently, copper(II) chelating compounds can counteract these toxic effects of copper dyshomeostasis in AD. Besides simple copper(II) chelators, copper(II) complexes with hybrid compounds containing salicylaldehyde based Schiff bases and benzothiazole [14], bis(thiosemicarbazones) [17,18] or 7-chloro-4-aminoquinoline Schiff bases [19] have also been studied as candidate therapeutic compounds for the treatment of AD. On the one hand, it has been suggested that these complexes may offer stronger inhibition of the  $\text{A}\beta$  peptide aggregation than simple ligands due to a combined multivalent effect against  $\text{A}\beta$  peptide. In addition, copper(II) complexes may offer significant antioxidant capacity contributing to the reduction of intracellular ROS and the increase of cell viability [14]. On the other hand, some copper(II) complexes may regulate intracellular delivery of copper [18]. In particular, when neutral stable lipophilic complexes of square planar geometry are exposed to the intracellular reducing environment,  $\text{Cu}^{\text{II}}$  is reduced to  $\text{Cu}^{\text{I}}$  and is then released by the ligand increasing copper bioavailability. As a result, several cell signaling pathways are activated, which, via GSK-3 $\beta$  phosphorylation, reduce  $\text{A}\beta$  peptide aggregation and Tau protein phosphorylation [17,18]. Furthermore, increase of copper bioavailability by these complexes may activate superoxide dismutase (SOD), thus reducing the toxic effect of oxidative stress [12,17,18]. These results indicate that further studies investigating the effect of the isolated copper(II) chelators and their complexes are essential to clarify whether copper can be converted from a risk factor into a beneficial tool for the treatment of AD.

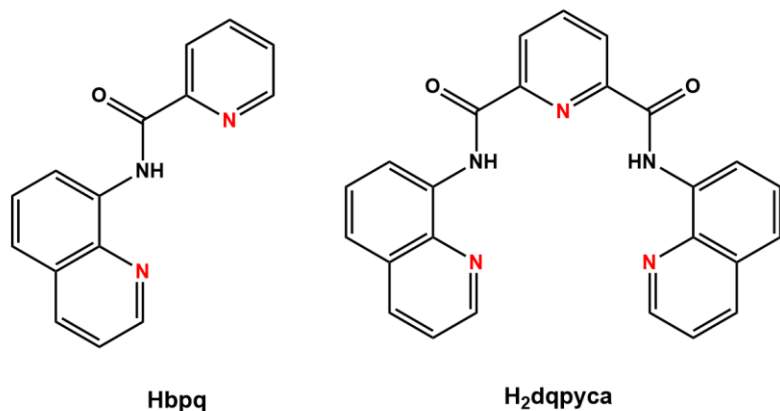
Currently, several research groups have focused on the synthesis and evaluation of metal chelators as a basis of multifunctional compounds [20–24]. Previous studies have described quinoline derivatives as promising compounds with positive results in preclinical models. For instance,

clioquinol (Scheme 1), a 8-hydroxyquinoline derivative, is a bidentate chelator, which binds to metal ions, mainly copper(II), and reduces A $\beta$  aggregation and oxidative stress [7,25,26]. In addition, several pyridine derivatives were shown to chelate metal ions, resulting in a reduction of metal-induced A $\beta$  aggregation, ROS production and the following toxicity [12].

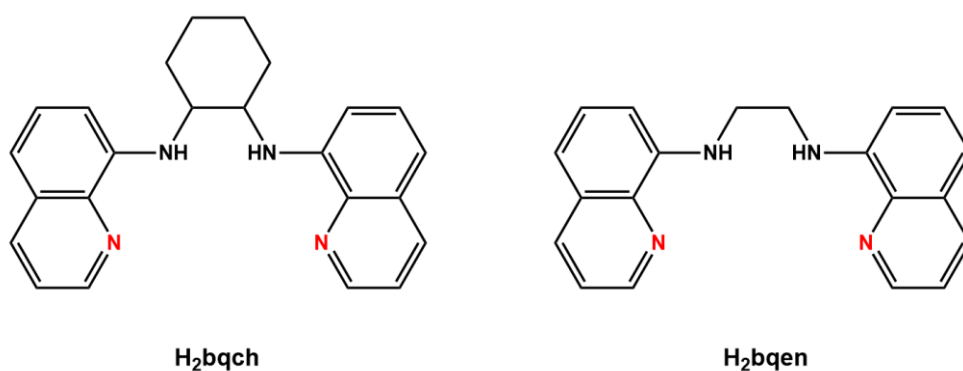


**Scheme 1.** Chemical structure of clioquinol.

Herein, we report on the synthesis and physicochemical characterization of copper(II) complexes with the ligands *N*-(8-quinolyl)pyridine-2-carboxamide (Hbpq) and *N*<sup>2</sup>,*N*<sup>6</sup>-di(quinolin-8-yl)pyridine-2,6-dicarboxamide (H<sub>2</sub>dqpyca) (Scheme 2), containing quinoline and pyridine rings, and the ligands *N,N'*-Bis(8-quinolyl)cyclohexane-1,2-diamine (H<sub>2</sub>bqch) and *N,N'*-Bis(8-quinolyl)ethane-1,2-diamine (H<sub>2</sub>bqen) (Scheme 3), containing quinoline rings. The ligands Hbpq and H<sub>2</sub>dqpyca (Scheme 2) have also the amide group(s) which is deprotonated quite easily upon interaction with Cu<sup>II</sup> and a very strong bond of Cu<sup>II</sup> with the deprotonated nitrogen is formed [27]. Furthermore, we studied the neuroprotective potential of the individual ligands and their copper(II) complexes against A $\beta$  peptide- and H<sub>2</sub>O<sub>2</sub>-induced cytotoxicity in human neuroblastoma SH-SY5Y cells. Two promising candidate compounds with minimal toxicity *in vitro* have been identified, that act protectively against A $\beta$  peptide- and/or H<sub>2</sub>O<sub>2</sub>-induced cell death, indicating that they could have the potential to be efficient multifunctional agents for the treatment of AD.



**Scheme 2.** The ligands Hbpq and H<sub>2</sub>dqpyca, containing quinoline and pyridine rings.



**Scheme 3.** The ligands H<sub>2</sub>bqch and H<sub>2</sub>bqen, containing quinoline rings.

## 2. Experimental section

### 2.1 General procedures and materials

All chemicals were obtained commercially and used without further purification. <sup>1</sup>H NMR spectra of the organic molecules were recorded on a Bruker Avance 300 spectrometer at 300 MHz. Merck silica gel 60 F<sub>254</sub> TLC plates were used for thin layer chromatography. Elemental analyses were determined by the microanalysis services of the School of Chemistry in Glasgow, using an EA 1110 CHNS, CE-440 Elemental Analyzer. Dulbecco's Modified Eagle's Medium (DMEM) and Ham's F-12 Nutrient Mixture were purchased from Gibco (Grand Island, NY, USA). Human neuroblastoma

SH-SY5Y cell line was kindly provided by Dr Th. Michailidis (University of Ioannina, Ioannina, Greece). 7PA2-CHO cells, which were isolated in the laboratory of Dr D. Selkoe (Harvard University, Boston, USA), were kindly provided by Dr K. Vekrellis (BRFAA, Athens, Greece). For cell viability assays, CellTiter 96<sup>®</sup> AQueous One Solution Reagent (G3581) containing a novel tetrazolium compound, [3-(4,5-dimethylthiazol-2-yl)-5-(3-carboxymethoxyphenyl)-2-(4-sulfophenyl)-2H-tetrazolium, inner salt (MTS)], and an electron coupling reagent, phenazine ethosulfate (PES), was purchased from Promega (Madison, WI, USA). The tested compounds were dissolved in DMSO in 0.25-50 mM stock solutions. Stock solutions were stored at -20°C. Final concentration of DMSO (vehicle) in biological studies was 0.2% v/v.

## 2.2 Chemical synthesis and crystallography

### 2.2.1 Chemical synthesis and characterization

***N*-(8-quinolyl)pyridine-2-carboxamide (Hbpq).** Pyridine-2-carboxylic acid (2.000 g, 16.24 mmol) and 8-aminoquinoline (2.342 g, 16.24 mmol) were suspended in pyridine (30 ml). The mixture was heated at 40°C for 10 min, triphenylphosphite (5.040 g, 16.24 mmol) was added dropwise and the mixture was stirred at reflux for 4 h. After cooling to room temperature, the volume of the solution was reduced to 5 ml and ice cold EtOH (10 ml) was added dropwise to the solution, until a white precipitate was formed. The precipitate was filtered off, washed multiple times with ice cold EtOH and diethyl ether and dried in vacuum. Yield: 76%. Anal. Calcd for C<sub>15</sub>H<sub>11</sub>N<sub>3</sub>O (Mr=249.27): C, 72.28; H, 4.45; N, 16.86. Found: C, 71.98; H, 4.51; N, 16.89. <sup>1</sup>H NMR (CDCl<sub>3</sub>): δ 12.28 (s, 1 H), 9.02-9.01 (m, 2 H), 8.83-8.82 (m, 1 H), 8.39-8.38 (d, 1 H), 8.24-8.22 (m, 1 H), 7.96 (m, 1 H), 7.62 (m, 2 H), 7.53 (m, 2 H) (Fig. S1A). [HR-ESI(+)-MS]: calcd for (C<sub>15</sub>H<sub>11</sub>N<sub>3</sub>ONa) {[M + Na]<sup>+</sup>} m/z 272.0794, found 272.0788 (100%). mp=123-124°C. R<sub>f</sub>=0.1 (chloroform:*n*-hexane, 1:1).

***N*<sup>2</sup>,*N*<sup>6</sup>-di(quinolin-8-yl)pyridine-2,6-dicarboxamide (H<sub>2</sub>dqpyca).** To a stirred solution of 2,6-pyridinedicarboxylic acid (3.000 g, 18 mmol) in pyridine (60 ml), solid 8-aminoquinoline (5.190 g, 36

mmol) in one portion and triphenylphosphite (9.60 ml, 36 mmol) were successively added and the mixture was refluxed overnight. The resulting solution was cooled to  $-18^{\circ}\text{C}$  overnight and the light yellow solid was filtered off, washed with cold ethanol (2 x 10 ml) and diethyl ether (2 x 10 ml) and dried in vacuum to afford 6.811 g of a white solid. Yield: 90% (based on the 2,6-pyridinedicarboxylic acid). Anal. calcd for  $\text{C}_{25}\text{H}_{17}\text{N}_5\text{O}_2$  ( $M_r=419.44$ ): C, 71.59; H, 4.09; N, 16.69. Found: C, 71.32; H, 4.18; N, 16.44.  $^1\text{H NMR}$  ( $\text{CDCl}_3$ ):  $\delta$  12.35 (s, 2H), 9.02-8.99 (dd, 2H), 8.57 (d, 2H), 8.25-8.16 (m, 5H), 7.68-7.60 (m, 4H), 7.34-7.30 (m, 2H) (Fig. S1B). [HR-ESI(+)-MS]: calcd for ( $\text{C}_{25}\text{H}_{18}\text{N}_5\text{O}_2$ )  $\{[\text{M} + \text{H}]^+\}$   $m/z$  420.1455, found 420.1443 (100%). mp= $286^{\circ}\text{C}$ .  $R_f=0.28$  (chloroform:*n*-hexane, 4:1).

#### ***N,N'*-Bis(8-quinolyl)cyclohexane-1,2-diamine (H2bqch).**

This compound was synthesized according to literature [28] at similar yield.  $^1\text{H NMR}$  ( $\text{CDCl}_3$ ):  $\delta$  8.57 (d, 2H), 7.98 (d, 2H), 7.32 (m, 4H), 6.98 (d, 2H), 6.82 (d, 2H), 6.41 (d, 2H), 3.77 (m, 2H), 2.41 (m, 2H), 1.86 (m, 2H), 1.56 (m, 4H) (Fig. S1C).

#### ***N,N'*-Bis(8-quinolyl)ethane-1,2-diamine (H2bqen).**

This compound was synthesized according to literature [28] at similar yield.  $^1\text{H NMR}$  ( $\text{CDCl}_3$ ):  $\delta$  8.70 (d, 2H), 8.06 (d, 2H), 7.39 (m, 4H), 6.78 (d, 2H), 6.44 (s, 2H), 3.76 (s, 4H) (Fig. S1D).

**[*N*-(quinolin-8-yl)pyridine-2-carboxamido-*N*<sup>1</sup>,*N*<sup>2</sup>,*N*<sup>3</sup>](chlorido)(methyl alcohol-*O*)copper(II), [ $\text{Cu}^{\text{II}}(\text{bpq})\text{Cl}(\text{HOCH}_3)$ ] (**1**).**  $\text{CuCl}_2 \cdot 2\text{H}_2\text{O}$  (0.068 g, 0.40 mmol) was dissolved in methyl alcohol under magnetic stirring. Solid Hbpq (0.100 g, 0.40 mmol) was added to the stirred solution in one portion and the mixture was stirred at room temperature for 3 h. The resulting green precipitate was filtered off, washed with diethyl ether (2 x 5 ml) and dried in vacuum. Yield: 76%. Anal. Calcd. for  $\text{C}_{16}\text{H}_{14}\text{N}_3\text{O}_2\text{CuCl}$  ( $M_r=379.30$ ): C, 50.66; H, 3.72; N, 11.08. Found: C, 50.70; H, 3.80; N, 11.05. Efforts to get crystals of **1** suitable for single crystal X-ray structure analysis were unsuccessful and thus,  $\text{Cu}(\text{ClO}_4)_2 \cdot 6\text{H}_2\text{O}$  was used as a source of copper(II) to get compound [ $\text{Cu}^{\text{II}}(\text{bpq})(\text{ClO}_4)(\text{HOCH}_3)$ ] (**1'**) as a green solid in 89% yield. Anal. Calcd. for  $\text{C}_{16}\text{H}_{14}\text{N}_3\text{O}_6\text{CuCl}$  (**1'**,  $M_r = 443.30$ ): C, 43.35; H, 3.18;

N, 9.48. Found: C, 43.32; H, 3.20; N, 9.51. The resulting green solid was dissolved in acetonitrile and layered with diethyl ether to obtain green crystals of  $[\text{Cu}^{\text{II}}(\text{bpq})(\text{ClO}_4)(\text{CH}_3\text{CN})]$  (**1''**) (Fig. 1A).

**Bis[ $\mu_2$ - $N^2, N^6$ -di(quinolin-8-yl)pyridine-2,6-dicarboxamido]dicopper(II),  $[\text{Cu}^{\text{II}}_2(\mu_2\text{dqpyca})_2]$  (**2**).**

$\text{Cu}^{\text{II}}(\text{CH}_3\text{COO})_2 \cdot \text{H}_2\text{O}$  (0.119 g, 0.60 mmol) was dissolved in ethyl alcohol (20 ml) under magnetic stirring. Solid  $\text{H}_2\text{dqpyca}$  (0.250 g, 0.60 mmol) was added to the stirred solution in one portion and the mixture was refluxed overnight. The color of the solution changed slowly to green and a green precipitate was formed. The resulting mixture was first cooled to room temperature and then to  $2^\circ\text{C}$ . The green precipitate was filtered off, washed with cold ethyl alcohol (2 x 3 ml) and diethyl ether (2 x 5 ml) and dried in vacuum. Yield: 73% (based on  $\text{H}_2\text{dqpyca}$ ). Anal. calcd for  $\text{Cu}_2\text{C}_{50}\text{H}_{30}\text{N}_{10}\text{O}_4$  ( $M_r=961.93$ ): C, 62.43; H, 3.14; N, 14.56. Found: C, 62.29; H, 3.27; N, 14.24.

Crystals of **2** suitable for X-ray diffraction analysis were obtained by layering diethyl ether into a concentrated chloroform solution of **2** (Fig. 1B).

**[ $N, N'$ -Bis(8-quinolyl)cyclohexane-1,2-diamine](dichlorido)copper(II),  $[\text{Cu}^{\text{II}}(\text{H}_2\text{bqch})\text{Cl}_2] \cdot 3\text{H}_2\text{O}$  (**3**).**

$\text{CuCl}_2 \cdot 2\text{H}_2\text{O}$  (0.046 g, 0.27 mmol) was dissolved in methyl alcohol under magnetic stirring. Solid  $\text{H}_2\text{bqch}$  (0.100 g, 0.27 mmol) was added to the stirred solution in one portion and the mixture was stirred at room temperature for 3 h. The resulting dark green precipitate was filtered off, washed with diethyl ether (2 x 5 ml) and dried in vacuum. Yield: 53%. Anal. Calcd. for  $\text{C}_{24}\text{H}_{30}\text{N}_4\text{O}_3\text{CuCl}_2$  ( $M_r=556.74$ ): C, 51.78; H, 5.43; N, 10.06. Found: C, 51.81; H, 5.45; N, 10.01. Efforts to get crystals of **3** suitable for single crystal X-ray structure analysis were unsuccessful and thus,  $\text{Cu}(\text{ClO}_4)_2 \cdot 6\text{H}_2\text{O}$  was used as a source of copper(II) to get a green solid. The resulting green solid was dissolved in acetonitrile and layered with diethyl ether to obtain green crystals of *trans*- $[\text{Cu}^{\text{II}}(\text{H}_2\text{bqch})(\text{ClO}_4)_2]$  (**3'**) (Fig. 1C).

**[N,N'-Bis(8-quinolyl)ethane-1,2-diamine](dichlorido)copper(II), [Cu<sup>II</sup>(H<sub>2</sub>bqen)Cl<sub>2</sub>]·H<sub>2</sub>O (4).**

Compound **4** was synthesized in the same way as **3**, using H<sub>2</sub>bqen instead of H<sub>2</sub>bqch. Yield 64%. Anal. Calcd. for C<sub>20</sub>H<sub>20</sub>N<sub>4</sub>OCuCl<sub>2</sub> (Mr=466.66): C, 51.48; H, 4.32; N, 12.01. Found: C, 51.71; H, 3.85; N, 12.80.

### 2.2.2 X-ray crystallographic data collection and structure refinement

Suitable single crystal was selected and mounted onto a rubber loop using Fomblin oil. Single-crystal X-ray diffraction data of **1''** were recorded on a Bruker Apex CCD diffractometer ( $\lambda$  (MoK $\alpha$ )=0.71073 Å) at 150 K equipped with a graphite monochromator. Structure solution and refinement were carried out with SHELXS-97 [29] and SHELXL-97 [30] using the WinGX software package [31]. Data collection and reduction were performed using the Apex2 software package. Corrections for incident and diffracted beam absorption effects were applied using empirical absorption corrections [32]. All the non-H atoms were refined anisotropically. The positions of hydrogen atoms were calculated based on stereochemical considerations using the riding model. Final unit cell data and refinement statistics for compound **1''** are collated in Table 1. The crystallographic data for compound **1''** (CCDC- 2017545) can be obtained free of charge from the Cambridge Crystallographic Data Centre, (12 Union Road, Cambridge CB2 1EZ; fax: (+44) 1223- 336-033; email: [deposit@ccdc.cam.ac.uk](mailto:deposit@ccdc.cam.ac.uk)).

**Table 1.** Crystallographic and experimental data for **1''**

<b>parameter</b>	
Empirical formula	C <sub>34</sub> H <sub>26</sub> Cl <sub>2</sub> Cu <sub>2</sub> N <sub>8</sub> O <sub>10</sub>
Formula weight	904.63
Temperature	150 K
Wavelength	0.71073 Å
Cryst. syst.	Monoclinic
Space group	P 21/n
α (Å)	7.669 (2)
b (Å)	17.100 (4)
c (Å)	13.359 (4)
α (deg)	90
β (deg)	91.636 (3)
γ (deg)	90
Vol. (Å <sup>3</sup> )	1751.2 (8)
Z	2
D <sub>calcd</sub> (Mg/m <sup>3</sup> )	1.716
Abscoeff (mm <sup>-1</sup> )	1.440
Theta (max)	26.498
Tmin	0.841
Tmax	0.931
Nref	3634
R, wR (all data)	0.0299, 0.0772

### 2.3 Pharmacological evaluation

#### 2.3.1 Cell culture and differentiation of SH-SY5Y cells

SH-SY5Y cells (P37-P42) were maintained in a growth medium consisting of DMEM:F12 (1:1) supplemented with 10% FBS, 1% P/S and L-glutamine (at a final concentration of 2 mM) and were incubated at 37°C and 5% CO<sub>2</sub>. Cell viability/cell death experiments were performed in 96-well plates with undifferentiated (at a seeding density of 3 X 10<sup>4</sup> cells/well) and differentiated cells (at a seeding density of 7.5 X 10<sup>4</sup> cells/well). Differentiation was induced by culturing cells in DMEM:F12 (1:1) supplemented with 0.1% FBS, 1% P/S, L-glutamine (at a final concentration of 2 mM) and retinoic acid (RA) 5 μM for at least 96 h. Differentiation medium was changed every 48 h.

### 2.3.2 Culture supernatant isolation from 7PA2-CHO cells

7PA2-CHO cells were cultured in 10 cm plates in a growth medium DMEM supplemented with 10% FBS, 1% P/S, L-glutamine (at a final concentration of 2 mM) and 100 µg/ml G418 to enrich for mutant APP-expressing cells. After two passages, they were shifted to medium without G418 for at least 24 h and after extensive washing, they were incubated in 10 ml of DMEM:F12 (1:1) medium supplemented with 1% P/S and L-glutamine (at a final concentration of 2 mM) for at least 16 h. The cell supernatant, containing secreted APP and a mixture of pathological A $\beta$  peptides in oligomeric forms [33], was collected and centrifuged to remove cells and cell debris. The final cleared supernatant was aliquoted and stored at -20°C. The same protocol was followed for the isolation of control supernatant from naïve CHO cells (CHO-K1) without the inclusion of G418.

### 2.3.3 Toxicity assays

Undifferentiated SH-SY5Y cells ( $3 \times 10^4$  cells/well) were cultured in 96-well plates. After 24 h, medium was changed to DMEM:F12 (1:1) supplemented with 1% P/S and L-glutamine (at a final concentration of 2 mM) but without FBS and compounds at various concentrations or vehicle (DMSO at a final concentration of 0.2% v/v) were added. Cell viability was assessed after 48 h by the MTS assay.

### 2.3.4 Neuroprotective effect of compounds against 7PA2-CHO supernatant and H<sub>2</sub>O<sub>2</sub>

Undifferentiated SH-SY5Y cells ( $3 \times 10^4$  cells/well) were seeded in 96-well plates in DMEM:F12 (1:1) medium supplemented with 10% FBS, 1% P/S and L-glutamine (at a final concentration of 2 mM) and were incubated at 37°C and 5% CO<sub>2</sub> for 24 h. Growth medium was aspirated, cells were washed with PBS and pre-incubated for 4.5 h in DMEM:F12 (1:1) medium in the presence of various concentrations of compounds or vehicle (DMSO). Subsequently, H<sub>2</sub>O<sub>2</sub> (final concentration 750 µM), 7PA2-CHO supernatant (final concentration 75% v/v) or CHO-K1 control supernatant (final concentration 75% v/v) was added. In the experiments with differentiated SH-SY5Y cells ( $7.5 \times 10^4$

cells/well), differentiation was performed before pre-incubation with the compounds. Cell viability was assessed after 48 h by the MTS assay.

### 2.3.5 Assessment of cell viability by the MTS assay

MTS reagent (20  $\mu$ l of a solution 1.90 mg/ml MTS and 300  $\mu$ M PES in Dulbecco's PBS, pH 6.0) was added to control and treated SH-SY5Y cells (total volume 120  $\mu$ l) in 96-well plates and the plates were incubated at 37°C and 5% CO<sub>2</sub> for 90 min. Absorption was measured in an ELISA spectrophotometer at 492 nm. All MTS assays were performed in triplicate samples in each experiment. Results are expressed as % cell viability with DMSO- or medium-treated cells (controls) representing 100% cell viability.

### 2.3.6 Molecular docking studies

Molecular docking studies of the synthesized metal chelators were performed using AutoDockTools-1.5.6 and the crystal structure of the complex AChE-rivastigmine (PDB ID:1GQR) as a template. The structures of Hbpq and H<sub>2</sub>dqpyca were taken from Pubchem database as SDF files while the structures of H<sub>2</sub>bqch and H<sub>2</sub>bqen were designed with ChemDraw, energy minimization was performed and they were exported as PDB files. A grid box was defined containing all critical amino acids of AChE which interact with rivastigmine, specifically residues Trp84, Gly118, Gly119, Glu199, Ser200, Ala201, Phe288, Phe290, Glu327, Phe330 and His440. Molecular docking studies of each chelator were performed and files with the energies of their various poses during their interaction with AChE and their PDBQT files were taken. Analysis of these interactions and bond distances for their best pose was performed using Pymol. Interactions of the chelators with the residues of AChE within 4 Å from the ligand binding site were tested. For each docking study a total of 9 docking poses were retained. These poses of each metal chelator appeared to be clustered in a single pose as the maximum energy difference between the most stable and the least stable poses ranged from 1.1 to 2.4 kcal/mol depending on the metal chelator (Table S1).

### 2.3.7 Statistical analysis

All experiments were repeated at least two times with different cell batches in triplicate samples. All data were expressed as means $\pm$ SEM with results pooled from all experiments. Calculation of EC<sub>50</sub> values was performed using the log(agonist) vs response-variable slope mode of Prism GraphPad. Statistical analysis between multiple groups was performed by ANOVA followed by Bonferroni post-hoc test using Prism GraphPad. \* corresponds to  $0.01 < p < 0.05$ , \*\* correspond to  $0.001 < p < 0.01$  and \*\*\* correspond to  $p < 0.001$ .



### 3.1.2 X-ray crystallography

The molecular structure of compound **1''** [ $\text{Cu}^{\text{II}}(\text{bpq})(\text{ClO}_4)(\text{CH}_3\text{CN})$ ] is depicted in Fig. 1A and selected bond lengths and angles are listed in Table 2. The metal center is surrounded by four different types of nitrogen donor atoms,  $\text{N}_{(\text{pyr})}$ ,  $\text{N}_{(\text{quin})}$ ,  $\text{N}_{(\text{amide})}$ ,  $\text{N}_{(\text{CH}_3\text{CN})}$  and an oxygen atom from the perchlorate ion. The copper(II) ion adopts a distorted square-pyramidal coordination geometry ( $\tau=0.24$ ) [34] with the oxygen atom occupying the axial positions and the nitrogen atoms occupying the equatorial plane. The  $\text{Cu}^{\text{II}}\text{-N}_{(\text{amide})}$  bond is the shortest (1.9'30 (2) Å) of all  $\text{Cu}^{\text{II}}\text{-N}$  bonds, which is consistent with literature values [35–37]. The  $\text{Cu}^{\text{II}}\text{-N}_{(\text{ACN})}$  bond (1.975 (2) Å) is shorter than the  $\text{Cu}^{\text{II}}\text{-N}_{(\text{pyr})}$  (2.003 (2) Å) and  $\text{Cu}^{\text{II}}\text{-N}_{(\text{quin})}$  (2.011 (2) Å) bonds and the  $\text{Cu}^{\text{II}}\text{-O}_{(\text{perchlorate})}$  bond (2.527 (2) Å) is the longest, as expected. The crystal structures of **2** and **3'** have been previously discussed in detail [38,39]. The structures of **2** and **3'** differ from **1''** as the copper(II) ion in the former complexes adopts a distorted octahedral geometry while complex **2** differs from complex **3'** as it is a binuclear compound while **3'** is a mononuclear compound (Fig. 1).

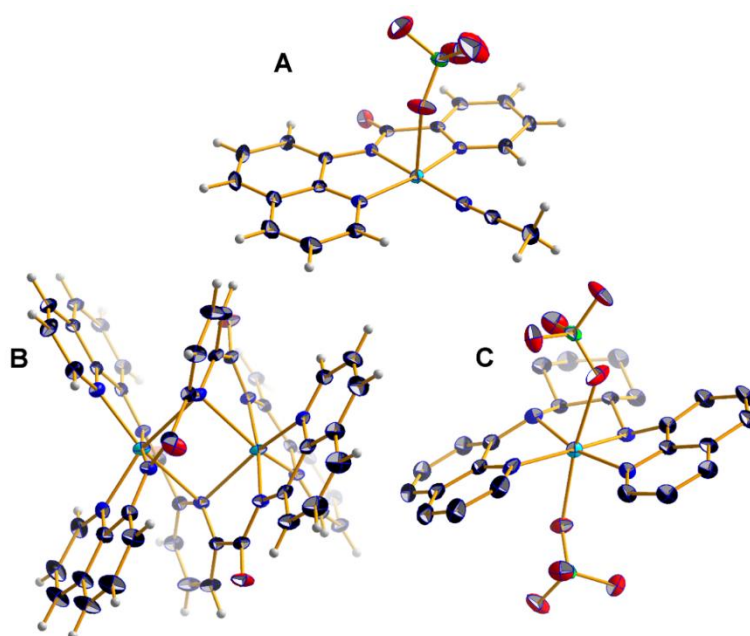


**Fig. 1.** Ball and stick representation of complexes **1''** (A), **2** (B) and **3'** (C).

**Table 2.** Interatomic distances (Å) and angles (deg) for **1'** relevant to the copper(II) coordination sphere.

parameter	Interatomic distances (Å) and angles (deg)
Cu (1) - O (2)	2.527 (2)
Cu (1) - N (1)	2.011 (2)
Cu (1) - N (2)	1.930 (2)
Cu (1) - N (3)	2.003 (2)
Cu (1) - N (4)	1.975 (2)
O (2) - Cu (1) - N (1)	92.00 (6)
O (2) - Cu (1) - N (2)	96.41 (6)
O (2) - Cu (1) - N (3)	92.70 (6)
O (2) - Cu (1) - N (4)	83.22 (6)
N (1) - Cu (1) - N (2)	82.58 (7)
N (1) - Cu (1) - N (3)	164.84 (7)
N (1) - Cu (1) - N (4)	96.93 (7)
N (2) - Cu (1) - N (3)	82.58 (7)
N (2) - Cu (1) - N (4)	179.38 (7)
N (3) - Cu (1) - N (4)	97.930 (7)

*Proposed structures of the copper(II) compounds 1, 3 and 4*

The proposed structures of compounds **1**, **3** and **4** (Scheme 4) are based on the solid-state (KBr discs) FT-IR spectra and their statistical analysis. In Figure 1 are shown the solid-state FT-IR spectra of the pair of compounds **3** and **3'** (i.e., the chloride and its perchlorate analogue respectively) in the low frequency region, the so-called fingerprint region.

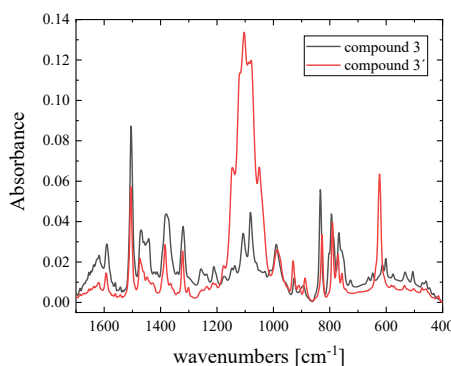


**Fig. 1** FT-IR spectra of compounds **3** and **3'** in the fingerprint region.

At a first glance, the spectra of compounds **3** and **3'** in the fingerprint region exhibit a resemblance implying characteristic structural similarities. As a general remark, we observe two spectral zones near  $600\text{ cm}^{-1}$  and  $1000\text{-}1200\text{ cm}^{-1}$  where the spectra differ significantly. These bands are assigned to vibrations of the coordinated perchlorate ion in **3'** [1].

Furthermore, the first derivatives of the spectra have been used to disentangle the pure vibrational density of states from the residual background slopes [2]. Indeed, a comparison of the first derivatives corresponding to the spectra of each compound (**3** with **3'**) reveals characteristic resemblance except for the spectral regions attributed to perchlorate species that have been discussed above.

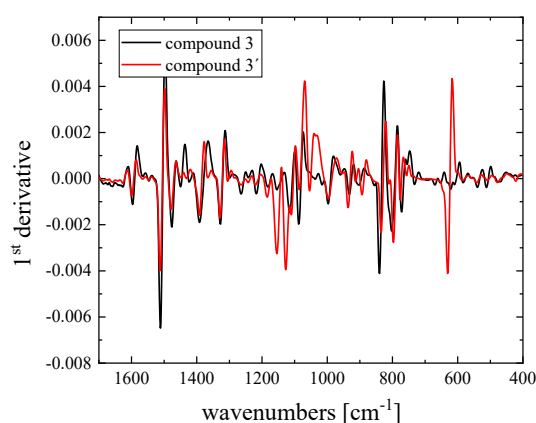


**Fig. 2** First derivative of the FT-IR spectra of compounds **3** and **3'** in the fingerprint region.

Additionally, the Pearson product-moment correlation (PPMC) has been used to follow the linear correlation between the spectra of each set presented in Fig. 1 in a quantitative manner [3]. In Fig. 3 are shown the confidence ellipses for the set of spectra presented in Fig. 1, respectively. In this Figure, the confidence ellipse includes points of the scatter matrix with correlation higher than 95%. Each point of the IR spectrum is represented by a point of the scatter matrix. It seems that for **3** and **3'** most of the points are inside confidence ellipse indicating spectral similarities. The spectral differences due

to the bands of perchlorate species and possible minor frequency shifts and bandwidth variations observed in the spectra are due to the different degree of interactions taking place in each compound.

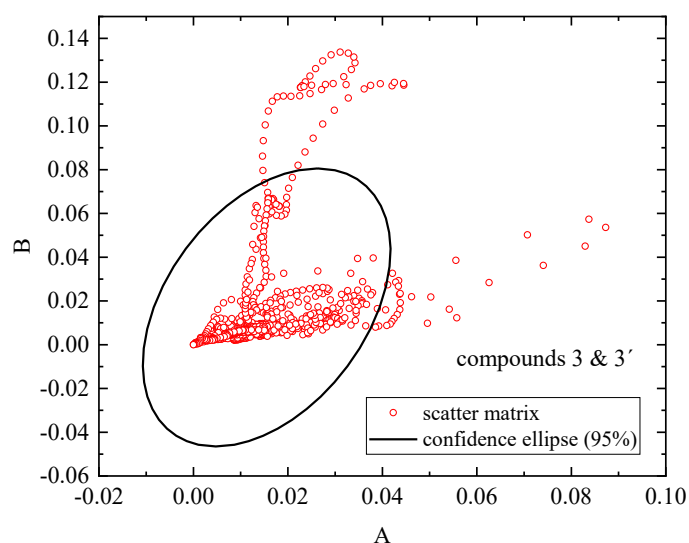


**Fig. 3** Confidence ellipse as obtained from Pearson-type correlation for the spectra presented in Fig. 1.

Finally, the 2-D correlation methodology has been used to further establish the structural similarity. The synchronous correlation map constructed from the vibrational spectra of the set is presented in Fig. 4. The synchronous 2-D maps exhibit concurrent variations, and the spectra are fully symmetric with respect to diagonal line [4]. This behavior is characteristic of a thorough spectral resemblance also implying a structural similarity. The peaks detected in the diagonal line are known as “auto-peaks”, while all the observed off-diagonal peaks are the “cross-peaks” and are related to synchronous spectral alterations with positive or negative intensities, respectively. The 2-D correlation spectral analysis provides an enhanced peak resolution by spreading the bands along the second dimension permitting thus a detailed evaluation of the structure [3-5].

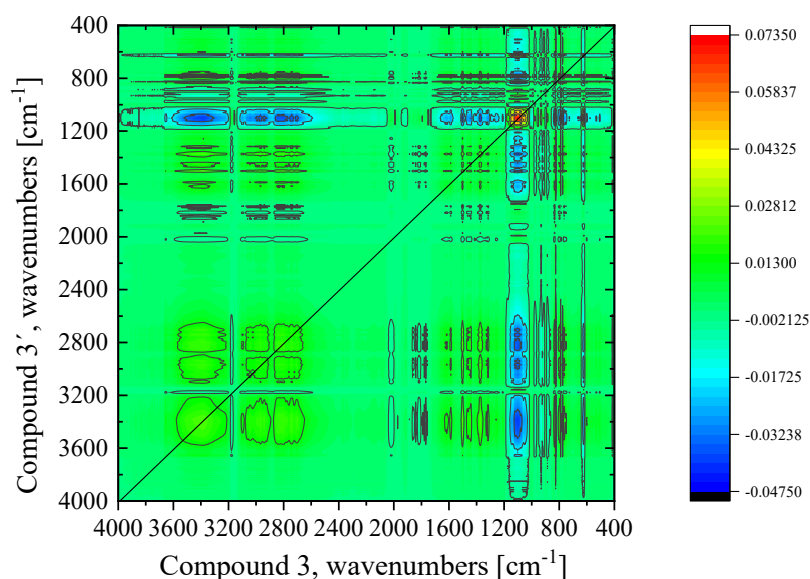


**Fig. 4** Synchronous 2-D correlation spectra constructed from the vibrational spectra of compound **3** and **3'**.

Thus, it is crystal-clear from all the above data the structures of compounds **3** and **3'** are very similar (see Scheme 4 and Figure 1). With the same reasoning, the structures of **1** and **4** are those reported in Scheme 4. (See supplementary material for more details and relevant graphs).

- 1) The infrared spectra of coordinated perchlorates, David L. Lewis, Eva Dixon Estes, Derek J. Hodgson, *Journal of Crystal and Molecular Structure*, volume 5, pages 67–74, 1975.
- 2) B. C. Smith, *Fundamentals of Fourier Transform Infrared Spectroscopy* (CRC Press, Taylor & Francis Group, 2<sup>nd</sup> edition, Boca Raton, USA, 2011).
- 3) I. Ketikidis, C. N. Banti, N. Kourkoumelis, C. G. Tsiafoulis, C. Papachristodoulou, A. G. Kalampounias, S. K. Hadjikakou, *Antibiotics* 2020, 9, 25; <http://dx.doi.org/10.3390/antibiotics9010025>

- 4) I. Noda, Y. Osaki, Two-dimensional Correlation Spectroscopy – Applications in Vibrational and Optical Spectroscopy (John Wiley & Sons Ltd, West Sussex, England, 2004).
- 5) A. G. Kalampounias, Correlating changes in structure and dynamical properties in LnX<sub>3</sub> (Ln = Y, Ho, Dy, Gd, Nd, La and X = Cl, Br) ionic melts, Chem. Pap. (2017) 71:1529-1539. DOI 10.1007/s11696-017-0147-2

### 3.2 Pharmacological evaluation

#### 3.2.1 Toxicity studies

The toxicity of compounds was examined in undifferentiated SH-SY5Y cells using the MTS assay after incubation for 48 h. The range of concentrations was selected from previous similar studies taking into account the solubility and toxicity concerns with metal chelators [19,21,40]. As shown in Fig. 2A, the metal chelator Hbpq displayed significant toxicity at concentrations  $\geq 10$   $\mu\text{M}$  with 60% cell death at 50  $\mu\text{M}$ . Its copper(II) complex **1** was extremely toxic even at a low concentration of 1  $\mu\text{M}$  resulting in almost 100% cell death (Fig. 2A). On the contrary, the metal chelator H<sub>2</sub>dqpyca and its copper(II) complex **2** were non-toxic at concentrations of 0.5-2  $\mu\text{M}$ , while only **2** at 10  $\mu\text{M}$  was significantly toxic (Fig. 2A). As for the metal chelators H<sub>2</sub>bqch, H<sub>2</sub>bqen and their copper(II) complexes **3-4** (Fig. 2B), they were found to be non-toxic at the indicated concentrations.

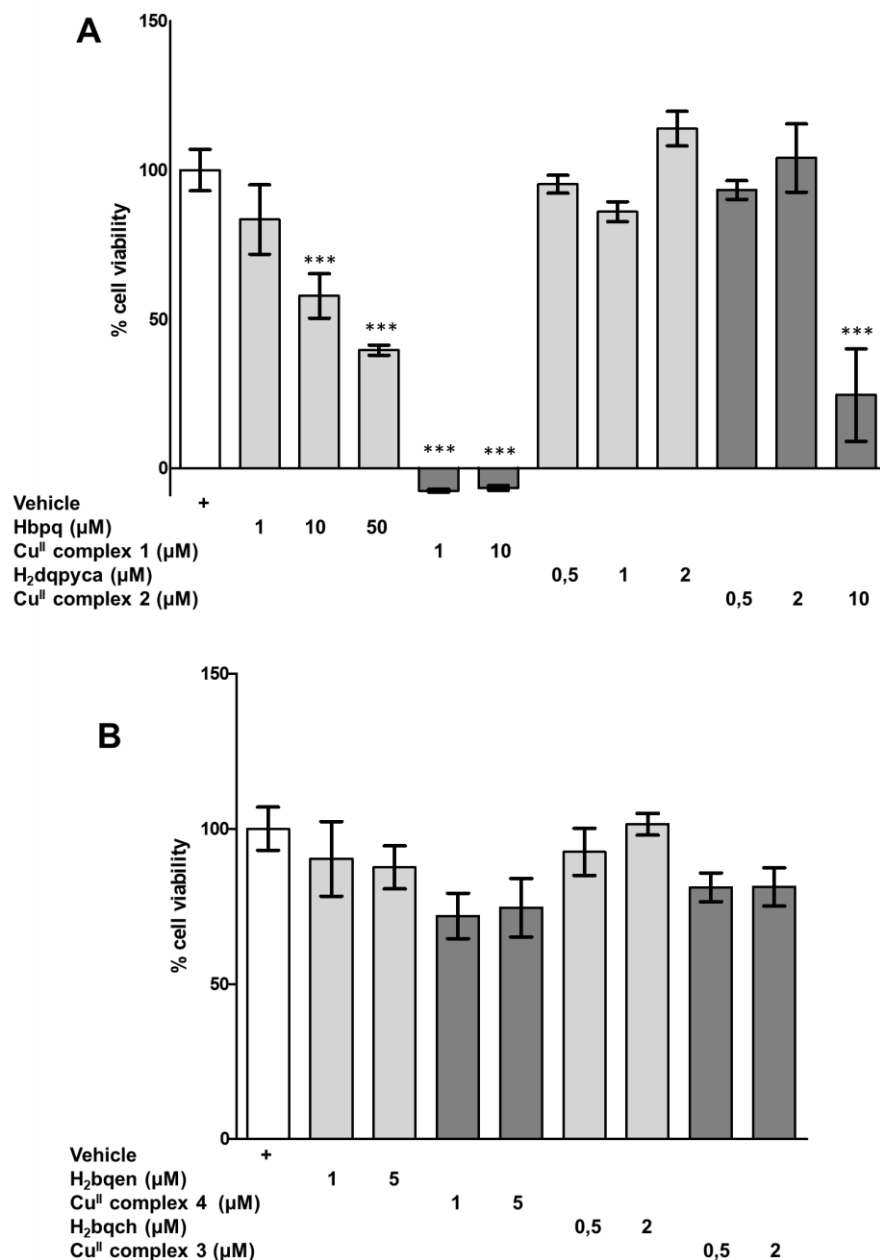


**Fig. 2.** Cytotoxicity of the metal chelators Hbpq, H<sub>2</sub>dqpyca (A), H<sub>2</sub>bqen, H<sub>2</sub>bqch (B) and their complexes with copper(II) in SH-SY5Y cells. Cells were treated with the compounds at various concentrations for 48 h. DMSO (vehicle) at a final concentration of 0.2% v/v was used as control. Cell viability was determined by the MTS assay. Data are expressed as means±SEM of at least two independent experiments in triplicate samples. Statistical analysis between multiple groups was performed by ANOVA followed by Bonferroni post-hoc test. Significance level \*\*\*p<0.001 as compared with vehicle.

The above results are in general agreement with other quinoline-based compounds previously studied. It has been suggested that 7-chloro-4-aminoquinoline Schiff bases [19], 8-hydroxyquinoline Schiff-base compounds [21], selenium-containing clioquinol derivatives [22], trehalose and glucose derivatives of 8-hydroxyquinoline [40] or other chelators, such as hybrid compounds of

salicylaldehyde based Schiff bases and benzothiazole [14] are generally non-toxic at concentrations  $\leq 5 \mu\text{M}$ . Certain copper(II) complexes have also been studied and were found to be either non-toxic [19,40] or slightly toxic (at  $10 \mu\text{M}$  concentrations in the presence of added  $\text{Cu}^{\text{II}}$ ) [41] in cell models. It should be noted here that combinatorial treatment of cells with chelators and copper(II) may not be appropriate for reporting toxicities of the chelator-copper(II) complex [41]. We administered the synthesized and characterized complexes directly to the cells as complexes and this approach better approximates the cellular condition. In this regard, it is important to highlight the results obtained with Hbpq and **1** (Fig. 2A). Hbpq, in contrast to  $\text{H}_2\text{dqpyca}$ , contains a single quinoline ring and is a tridentate chelator. At  $1 \mu\text{M}$  it is non-toxic while the formed copper(II) complex **1** at the same concentration kills almost all cells, exhibiting thus a far greater toxic effect under the same conditions. At equivalent concentrations,  $\text{H}_2\text{dqpyca}$ , which contains two quinoline rings and is a pentadentate chelator, and its copper(II) complex **2** are well-tolerated by cells. We conclude that the presence of only one single quinoline ring in a quinoline-based scaffold results in a metal chelator that when complexed with  $\text{Cu}^{\text{II}}$  exerts a dramatic toxic effect in cells. This toxic effect could be due to the fact that a tridentate chelator forms less stable complexes with copper(II) than a pentadentate chelator. So,  $\text{Cu}^{\text{II}}$  could be released more easily from **1** and activate proapoptotic pathways. Due to the high toxicity associated with Hbpq and its complex with  $\text{Cu}^{\text{II}}$  we didn't proceed in further experimentation with these compounds in this paper although it would be interesting to investigate in further detail the mechanisms of cell death induced by these compounds in the future.

### *3.2.2 Neuroprotective effects of compounds against 7PA2-CHO supernatant-induced toxicity in SH-SY5Y cells*

The amyloid hypothesis is one of the basic pathophysiological mechanisms related to AD.  $\text{A}\beta$  peptides in oligomeric forms of  $\text{A}\beta_{1-42}$  are produced by APP metabolism and are considered the primary toxic species [2,4]. In order to better approximate the in vivo condition of production of toxic  $\text{A}\beta$  species by APP metabolism, we utilized the 7PA2-CHO cell line developed by the Selkoe lab [42].

These cells stably express a form of APP with mutations found in patients with familial AD. Mutant APP is secreted in the medium and processed into several A $\beta$  peptides including the major toxic oligomeric forms [43]. In order to study the neuroprotective effects of synthesized metal chelators and their complexes with copper(II) we pre-incubated SH-SY5Y cells for 4.5 h with the indicated concentrations and then challenged cells with 7PA2-CHO supernatant containing toxic A $\beta$  peptide forms for 48 h. Cell viability was assessed by the MTS assay. In pilot experiments we characterized the dose-dependency of two different batches of 7PA2-CHO supernatant and reproducibly found that a concentration of 75% (v/v) resulted in 40-60% SH-SY5Y cell death. Incubation of cells with control CHO-K1 supernatant (from naïve CHO cells which do not express APP) did not result in any toxic effect and was used as control in these experiments.

As shown in Fig. 3A, compound H<sub>2</sub>dqpyca at both concentrations tested exerted a statistically significant strong neuroprotective effect against A $\beta$  peptide-induced SH-SY5Y cell death. The calculated neuroprotective effect was 50% at the concentration of 0.5  $\mu$ M, which however did not increase significantly at 2  $\mu$ M. In contrast, **2** did not show any statistically significant neuroprotective effect. Analysis of H<sub>2</sub>bqen showed a small neuroprotective effect at 1  $\mu$ M which however was not statistically significant and was abolished at 5  $\mu$ M (Fig. 3B). In sharp contrast, **4** at a concentration of 5  $\mu$ M was found to cause additive toxicity in the presence of A $\beta$  peptides with their combination resulting in almost 90% cell toxicity; this may suggest the generation of Cu<sup>II</sup> species by **4** that may stabilize or further enhance formation of A $\beta$  peptide oligomers and thus increase toxicity, a well-described aspect of the amyloid-metal hypothesis [2,4,7]. Of all compounds analyzed, H<sub>2</sub>bqch and its copper(II) complex **3** did not exhibit any significant neuroprotection nor additive toxic effect in the presence of toxic A $\beta$  peptides at the concentrations tested (Fig. 3B). So, we conclude that distinct copper(II) complexes with different affinities might work in opposite ways by increasing A $\beta$  toxicity.

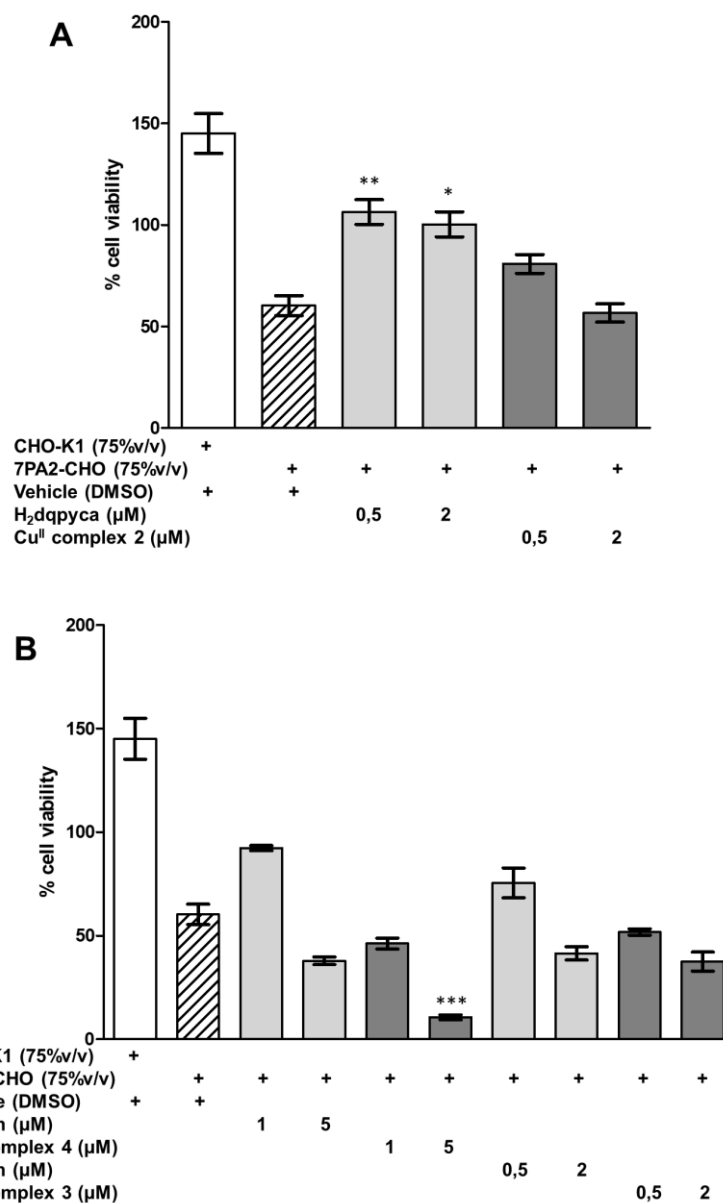


**Fig. 3.** Neuroprotective effect of the metal chelators H<sub>2</sub>dqpyca (A), H<sub>2</sub>bqen, H<sub>2</sub>bqch (B) and their complexes with copper(II) against 7PA2-CHO supernatant-induced toxicity in SH-SY5Y cells. Cells were pretreated with the compounds at the indicated concentrations for 4.5 h and then challenged with 75% v/v 7PA2-CHO supernatant for 48 h. DMSO (vehicle) and CHO-K1 supernatant (from naïve CHO cells) were used as controls. Cell viability was determined by the MTS assay. Data are expressed as means±SEM of two independent experiments in triplicate samples. Statistical analysis between multiple groups was performed by ANOVA followed by Bonferroni post-hoc test. Significance levels \*0.01<p<0.05, \*\*0.001<p<0.01, \*\*\*p<0.001 as compared with the 7PA2-CHO supernatant-treated cells.

### 3.2.3 Neuroprotective effects of compounds against H<sub>2</sub>O<sub>2</sub>-induced toxicity in SH-SY5Y cells

Oxidative stress is another basic mechanism related to AD and also highly relevant to the study of metal chelators. On the one hand, metal ions, especially excess copper(II), may increase A $\beta$  peptide

aggregation and ROS production thus contributing to cell death in AD [4]. In addition, many previously synthesized metal chelators have been found to be potent antioxidants [20,21]. On the other hand, increase of copper(II) availability in cells by certain copper(II) complexes may also act protectively reducing the toxic effect of oxidative stress [12,17,18]. For these reasons we extended our experiments to screen for possible neuroprotective effects of our synthesized metal chelators and complexes against H<sub>2</sub>O<sub>2</sub>-induced oxidative stress in SH-SY5Y cells. In preliminary experiments we established the dose-response curve of H<sub>2</sub>O<sub>2</sub>-induced toxicity and found an LD<sub>50</sub> value of approx. 700 μM. In all subsequent experiments we challenged SH-SY5Y cells with H<sub>2</sub>O<sub>2</sub> at 750 μM resulting in a reproducible 70-85% cell death effect after 48 h. As shown in Fig. 4A, H<sub>2</sub>dqpyca at 2 μM exhibited a neuroprotective effect, while **2** was ineffective. H<sub>2</sub>bqen and its complex with copper(II), as well as H<sub>2</sub>bqch were also largely ineffective (Fig. 4B). A prominent exception here was **3** which at 2 μM exerted a significant neuroprotective effect against H<sub>2</sub>O<sub>2</sub>-induced SH-SY5Y cell death and a similar trend was evident for a lower concentration of 0.5 μM (Fig. 4B).

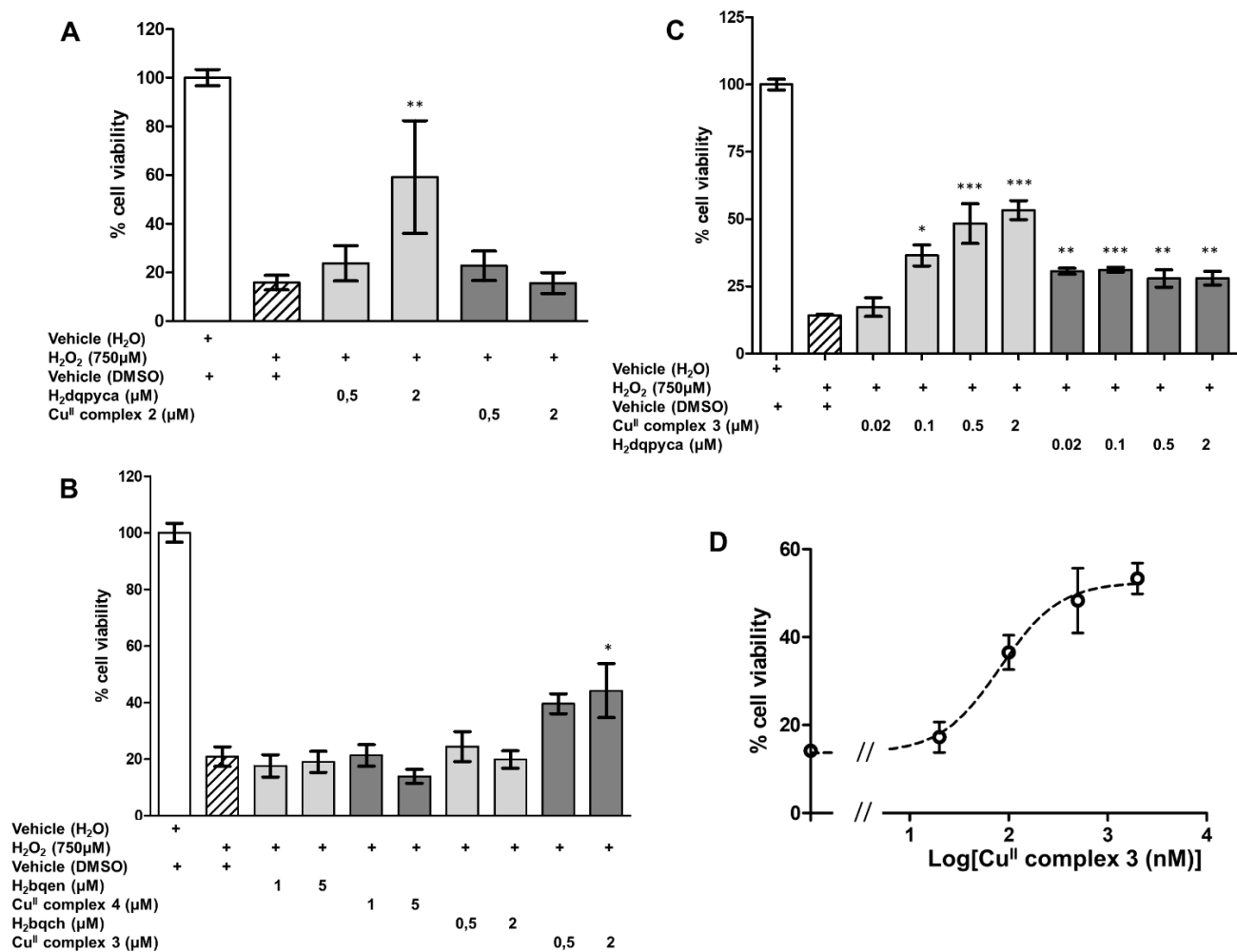


**Fig. 4.** Neuroprotective effect of the metal chelators H<sub>2</sub>dqpyca, H<sub>2</sub>bqen, H<sub>2</sub>bqch and their complexes with copper(II) against H<sub>2</sub>O<sub>2</sub>-induced toxicity in SH-SY5Y cells. (A), (B). Undifferentiated cells were pretreated with the compounds at the indicated concentrations for 4.5 h and then challenged with H<sub>2</sub>O<sub>2</sub> 750 μM for 48 h. DMSO and H<sub>2</sub>O (vehicles) were used as controls. Cell viability was determined by the MTS assay. Data are expressed as means±SEM of two independent experiments in triplicate samples. (C). Dose-dependent experiments of H<sub>2</sub>dqpyca and the copper(II) complex **3** in differentiated SH-SY5Y cells. Treatments with the indicated concentrations as above. Data are expressed as means±SEM of triplicate samples. (D). Dose-response curve for the copper(II) complex **3** neuroprotective effect used for determination of EC<sub>50</sub> value. Results were re-plotted from Fig. 4C. Statistical analysis between multiple groups was performed by ANOVA followed by Bonferroni post-hoc test. Significance levels \*0.01<p<0.05, \*\*0.001<p<0.01, \*\*\*p<0.001 as compared with the H<sub>2</sub>O<sub>2</sub>-treated cells.

### 3.2.4 Investigation of dose-dependent effects of compounds H<sub>2</sub>dqpyca and **3** in differentiated SH-SY5Y cells reveals differential modes of neuroprotection against H<sub>2</sub>O<sub>2</sub>-induced toxicity

Due to the promising neuroprotective effects against H<sub>2</sub>O<sub>2</sub>-induced cytotoxicity demonstrated by H<sub>2</sub>dqpyca and **3** in the first round of experiments, we decided to study in more detail these two

compounds. Of note, H<sub>2</sub>dqpyca was also found to be the most effective in protecting against A $\beta$  peptide-toxicity (Fig. 3A). **3**, on the other hand, was the only studied copper(II) complex that exerted a significant antioxidant effect (Fig. 4B) and was also virtually devoid of any additive toxic effect when co-administered with A $\beta$  peptides from 7PA2-CHO supernatant (Fig. 3B).

In order to better characterize these compounds, we performed dose-response neuroprotection experiments in differentiated SH-SY5Y cells. Differentiation was achieved with a modified retinoic acid-based protocol in order to enrich for the non-proliferating neurite-extending cells that exhibit a more mature neuron-like phenotype [44]. Morphological differentiation is accompanied by increased expression of neuronal markers and acquisition of a cholinergic neuron phenotype, more relevant to AD [44–47]. Pilot experiments for H<sub>2</sub>O<sub>2</sub>-induced cytotoxicity in differentiated SH-SY5Y cells revealed a similar to non-differentiated cells LD<sub>50</sub> value (data not shown). As shown in Fig. 4C, when differentiated SH-SY5Y cells were pre-incubated with a wider range of concentrations (0.02–2  $\mu$ M) of **3** and H<sub>2</sub>dqpyca and then challenged with H<sub>2</sub>O<sub>2</sub>, we observed a clear dose-dependent neuroprotective effect for **3**. The maximal neuroprotective effect of **3** was calculated at 35–40% with a logEC<sub>50</sub> value of 1.91 $\pm$ 0.16 (n=3) corresponding to an EC<sub>50</sub> concentration of approx. 80 nM (Fig. 4D). According to our knowledge, this is one of the lowest EC<sub>50</sub> values reported in the literature for cellular *in vitro* studies. The most significant effect of previously studied compounds accounted for a modest 3.4–28.7% increase in cell viability, with EC<sub>50</sub> values reported in the low to high micromolar range [48–51]. Surprisingly, H<sub>2</sub>dqpyca, although still caused a statistically significant neuroprotective effect against H<sub>2</sub>O<sub>2</sub>-induced toxicity in differentiated SH-SY5Y cells (15–20% increase of cell viability) (Fig. 4C), did not exhibit any clear dose-dependency. Apparently, this mode of action of H<sub>2</sub>dqpyca suggests a limiting, indirect, neuroprotective mechanism against oxidative stress (see Section 3.2.5, below). On the contrary, our detailed analysis highlights copper(II) complex **3**, which exhibits drug-like properties with nanomolar potency in protecting cells against oxidative stress, as a promising compound for further experimentation and development.

### *3.2.5 Molecular docking studies suggest possible interaction of the synthesized quinoline-based metal chelators with acetylcholinesterase active site*

We were intrigued by the absence of a dose-dependent neuroprotective effect of H<sub>2</sub>dqpyca against H<sub>2</sub>O<sub>2</sub>-induced toxicity (Fig. 4C). At the same time, H<sub>2</sub>dqpyca was found to be the most effective compound in protecting against A $\beta$  peptide-induced toxicity in our experiments (Fig. 3A). Given that it is likely also a BBB permeable molecule as predicted by multiple algorithms testing BBB permeability (data not shown), and hence a promising compound to study further, we pursued an additional line of experimentation to probe for the possible mechanism of action for H<sub>2</sub>dqpyca. Acetylcholinesterase, the main target of current AD drugs, is also involved indirectly in the A $\beta$  and oxidative stress hypotheses of AD. For example, A $\beta$  peptide aggregation is promoted by AChE via its peripheral anionic site (PAS) [52–54], while, oxidative stress may alter the levels and/or activity of AChE directly or indirectly [55,56]. Interestingly, treatment of SH-SY5Y cells with H<sub>2</sub>O<sub>2</sub> results in allosteric activation of AChE characterized by an increase in  $V_{max}$  with no changes in  $K_m$  and, importantly, lack of dose-dependent effects of H<sub>2</sub>O<sub>2</sub> in culture [55]. Lack of dose-dependency has been also reported for the partial protection from H<sub>2</sub>O<sub>2</sub>-induced apoptosis by multifunctional AChE inhibitors [57,58]. Thus, we reasoned that lack of dose-dependency for the H<sub>2</sub>dqpyca neuroprotective effect against H<sub>2</sub>O<sub>2</sub> may be due to possible interaction with AChE.

In order to study the possibility of interactions with AChE, we performed molecular docking simulations using AutoDockTools-1.5.6 using the crystal structure of the AChE-Rivastigmine complex (PDB ID:1GQR) as a template [59,60]. We analyzed all metal chelators Hbpq, H<sub>2</sub>dqpyca, H<sub>2</sub>bqch and H<sub>2</sub>bqen in terms of interactions and bond distances with critical amino acids of AChE that interact also with rivastigmine [23,59]. Docking and the subsequent calculation of scores and free energies were performed using default parameters and are shown in Table S1. Interestingly, our analysis indicated that H<sub>2</sub>dqpyca strongly interacts with AChE, followed by H<sub>2</sub>bqch. These two metal chelators showed the lowest free energy values for the most stable conformations (Table S1). For

example, as shown in Fig. 5 and Table 3, H<sub>2</sub>dqpyca interacts with the PAS of AChE, forming hydrogen bonds between carbonyl oxygen and NH group of the ligand and Tyr70, Tyr121 and Tyr334 with a distance of 2.2 Å. In addition, electrostatic interactions are observed between carbonyl oxygen of H<sub>2</sub>dqpyca and Asp72. The quinoline moiety of H<sub>2</sub>dqpyca forms  $\pi$ - $\pi$  stacking interactions with Trp279 and van der Waals interactions with Phe290 at a distance of 3.7 Å. In addition, H<sub>2</sub>dqpyca via its quinoline moieties interacts with the catalytic active site (CAS) of AChE via electrostatic interactions with Glu199 and His440 at distances of 3.4 Å and 3.6 Å respectively.  $\pi$ - $\pi$  interactions are observed between quinoline and Trp84 with a distance of 3.5 Å while van der Waals interactions are formed with Gly118, Phe288 and Phe330 (distances of 3.7 Å, 3.1 Å and 3.5 Å respectively). Conclusively, H<sub>2</sub>dqpyca shows a similar type of interaction with rivastigmine possibly acting as an AChE inhibitor.

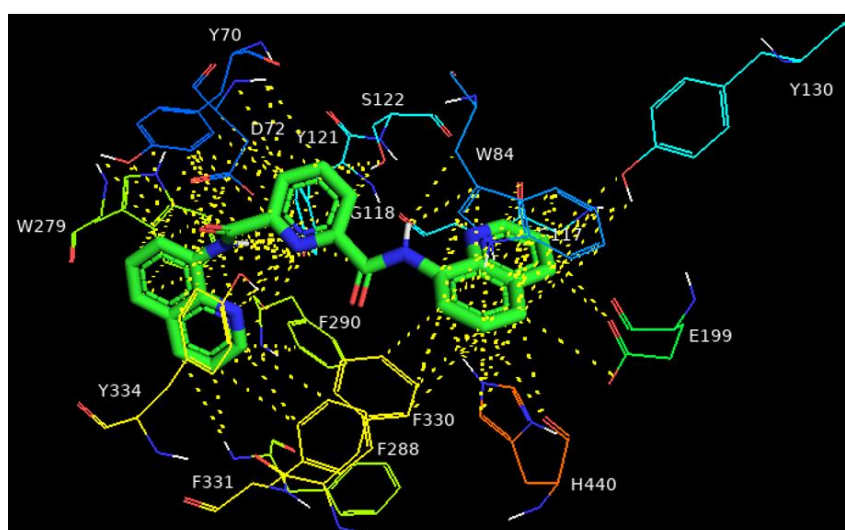


**Fig. 5.** Molecular docking simulation of the metal chelator H<sub>2</sub>dqpyca and the AChE-rivastigmine (PDB ID: 1GQR) binding site. Interactions of H<sub>2</sub>dqpyca (shown in green) with the critical amino acids of AChE. The dashed lines show hydrogen bonds and electrostatic,  $\pi$ - $\pi$  stacking and van der Waals interactions between the fragments of H<sub>2</sub>dqpyca and the critical amino acids of AChE.

**Table 3.** Bond interactions of H<sub>2</sub>dqpyca-AChE and bond distances.

<b>Bond</b>	<b>Distance (Å)</b>
Quinoline-Trp84	3.5
N <sub>quin</sub> -Gly118C <sub>A</sub>	3.9
C <sub>quin</sub> -Gly118C <sub>A</sub>	3.6
C <sub>quin</sub> -Gly118N	3.5
C <sub>quin</sub> -Gly118HN	3.9
C <sub>quin</sub> -Glu199O <sub>E1</sub>	3.2-3.6
C <sub>quin</sub> -Phe288HN	3.1
C <sub>quin</sub> -Phe290C <sub>E1</sub>	3.5-3.9
C <sub>quin</sub> -Phe330C <sub>E1</sub>	3.5
C <sub>quin</sub> -His440N <sub>E2</sub>	3.3-4
C <sub>quin</sub> -His440O	3.4-3.5

This result could explain the different levels of neuroprotection against A $\beta$  peptide- and H<sub>2</sub>O<sub>2</sub>-induced toxicities shown by H<sub>2</sub>dqpyca. Besides a direct effect, as a Cu<sup>II</sup> chelator, the high neuroprotection of H<sub>2</sub>dqpyca against A $\beta$  peptide-induced toxicity could be due to additional interactions with AChE resulting in direct inhibition and/or further A $\beta$  peptide disaggregation [24,54]. Similarly, the modest neuroprotective effect (15-20% increase of cell viability) against H<sub>2</sub>O<sub>2</sub>-induced toxicity in the absence of dose-dependency could be explained by protection only against the fixed H<sub>2</sub>O<sub>2</sub>-induced activation of AChE, described in SH-SY5Y cells under very similar conditions [55].

In addition to providing insight on the neuroprotective mechanisms of H<sub>2</sub>dqpyca, our molecular docking experiments highlight the possibility of an additional property for some of our quinoline derivatives as AChE interactors that may prove important for further experimentation and development.

#### 4. Conclusions

In conclusion, several quinoline derivatives (metal chelators) and their copper(II) complexes have been synthesized and physicochemically characterized. All of these compounds have also been pharmacologically evaluated. Our experiments provide significant insight into aspects of the pleiotropic neuroprotective actions of quinoline-based metal chelators and their copper(II) complexes against A $\beta$  peptide- and H<sub>2</sub>O<sub>2</sub>-induced toxicities in cells. We identified two compounds that exhibited favorable mechanistic and pharmacological properties. In particular, the metal chelator H<sub>2</sub>dqpyca showed significant neuroprotective effects against both A $\beta$  peptide- and H<sub>2</sub>O<sub>2</sub>-induced toxicities in SH-SY5Y neuroblastoma cells. Furthermore, using the acetylcholinesterase-rivastigmine crystal structure as a template, we found an increased possibility of interactions between the metal chelator H<sub>2</sub>dqpyca and AChE. According to our knowledge, this is the first demonstration of a quinoline-based ligand that possibly interacts with AChE and at the same time has direct pleiotropic neuroprotective activity against A $\beta$  and oxidative stress in cells. In addition, the copper(II) complex [Cu<sup>II</sup>(H<sub>2</sub>bqch)Cl<sub>2</sub>] $\cdot$ 3H<sub>2</sub>O revealed a potent dose-dependent neuroprotection against H<sub>2</sub>O<sub>2</sub>. Thus, we have identified two promising quinoline compounds, the metal chelator H<sub>2</sub>dqpyca and the copper(II) complex [Cu<sup>II</sup>(H<sub>2</sub>bqch)Cl<sub>2</sub>] $\cdot$ 3H<sub>2</sub>O, which should be developed further as multifunctional lead compounds targeting the AChE, amyloid, metal ion and oxidative stress related pathways involved in AD pathophysiology.

## Abbreviations

AD	Alzheimer's disease
AChE	acetylcholinesterase
CNS	central nervous system
A $\beta$	beta amyloid
NMDA	N-methyl-D-aspartate
APP	amyloid precursor protein
ROS	reactive oxygen species
GSK-3 $\beta$	glycogen synthase kinase-3 beta
SOD	superoxide dismutase
H <sub>2</sub> O <sub>2</sub>	hydrogen peroxide
NMR	nuclear magnetic resonance
TLC	thin layer chromatography
DMEM	Dulbecco's Modified Eagle's Medium
CHO	Chinese hamster ovary
MTS	3-(4,5-dimethylthiazol-2-yl)-5-(3-carboxymethoxyphenyl)-2-(4-sulfophenyl)-2H-tetrazolium, inner salt
PES	phenazine ethosulfate
HR-ESI(+)-MS	high-resolution electrospray ionization mass spectrometry
FBS	fetal bovine serum
RA	retinoic acid
EC <sub>50</sub>	half maximal effective concentration
LD <sub>50</sub>	median lethal dose
BBB	blood-brain barrier
PAS	peripheral anionic site
CAS	catalytic active site

## Author contributions

**Nikolaos Pavlidis:** Conceptualization, Validation, Formal analysis, Investigation, Data curation, Writing-original draft, Project administration. **Aristeidis Kofinas:** Validation, Formal analysis, Investigation, Data curation. **Michael G. Papanikolaou:** Validation, Formal analysis, Investigation, Data curation, Writing-original draft. **Haralampos N. Miras:** Validation, Formal analysis, Investigation, Data curation. **Chryssoula Drouza:** Validation, Formal analysis, Investigation, Data curation. **Angelos G. Kalampounias:** Validation, Spectral analysis, Investigation, Writing-original draft. **Themistoklis A. Kabanos:** Conceptualization, Writing-original draft, Writing-review and editing, Supervision, Project administration. **Maria Konstandi:** Conceptualization, Writing-review and editing, Supervision, Project administration. **George Leondaritis:** Conceptualization, Writing-original draft, Writing-review and editing, Supervision, Project administration.

## **Acknowledgements**

We thank Prof. Anastasios Keramidas (Department of Chemistry, University of Cyprus, Nicosia) for help with characterization of compounds and Drs. Chryssoula Petrokilidou and Nikolaos Kourkoumelis (Department of Medical Physics, Faculty of Medicine, University of Ioannina) for advice on molecular docking studies.

## **Funding**

NP was supported by a Bodossaki Foundation (Athens, Greece) Scholarship for postgraduate studies. The work was partially supported by IPIROS 2014-2020/no. E.E. 82474 grant (to MK).

## References

- [1] P. Adam, S. Křížková, Z. Heger, P. Babula, V. Pekařík, M. Vaculovičová, C.M. Gomes, R. Kizek, V. Adam, Metallothioneins in Prion-and Amyloid-Related Diseases, *J. Alzheimer's Dis.* 51 (2016) 637–656. <https://doi.org/10.3233/JAD-150984>.
- [2] K.P. Kepp, Alzheimer's disease: How metal ions define  $\beta$ -amyloid function, *Coord. Chem. Rev.* 351 (2017) 127–159. <https://doi.org/10.1016/j.ccr.2017.05.007>.
- [3] E. Karran, M. Mercken, B. De Strooper, The amyloid cascade hypothesis for Alzheimer's disease: An appraisal for the development of therapeutics, *Nat. Rev. Drug Discov.* 10 (2011) 698–712. <https://doi.org/10.1038/nrd3505>.
- [4] C. Cheignon, M. Tomas, D. Bonnefont-Rousselot, P. Faller, C. Hureau, F. Collin, Oxidative stress and the amyloid beta peptide in Alzheimer's disease, *Redox Biol.* 14 (2018) 450–464. <https://doi.org/10.1016/j.redox.2017.10.014>.
- [5] A. Pal, M. Siotto, R. Prasad, R. Squitti, Towards a unified vision of copper involvement in Alzheimer's disease: A review connecting basic, experimental, and clinical research, *J. Alzheimer's Dis.* 44 (2015) 343–354. <https://doi.org/10.3233/JAD-141194>.
- [6] W.H. Organisation, Dementia, (2019). <https://www.who.int/news-room/fact-sheets/detail/dementia> (accessed July 17, 2020).
- [7] K.P. Kepp, Bioinorganic chemistry of Alzheimer's disease, *Chem. Rev.* 112 (2012) 5193–5239. <https://doi.org/10.1021/cr300009x>.
- [8] S.D. Portbury, P.A. Adlard, Zinc signal in brain diseases, *Int. J. Mol. Sci.* 18 (2017) 2506. <https://doi.org/10.3390/ijms18122506>.
- [9] A. Contestabile, The history of the cholinergic hypothesis, *Behav. Brain Res.* 221 (2011) 334–340. <https://doi.org/10.1016/j.bbr.2009.12.044>.
- [10] K. Blennow, M.J. de Leon, H. Zetterberg, Alzheimer's disease, *Lancet.* 368 (2006) 387–403. [https://doi.org/10.1016/S0140-6736\(06\)69113-7](https://doi.org/10.1016/S0140-6736(06)69113-7).
- [11] I. Sotiropoulos, C. Catania, L.G. Pinto, R. Silva, G.E. Pollerberg, A. Takashima, N. Sousa, O.F.X. Almeida, Stress acts cumulatively to precipitate Alzheimer's disease-like tau pathology and cognitive deficits, *J. Neurosci.* 31 (2011) 7840–7847. <https://doi.org/10.1523/JNEUROSCI.0730-11.2011>.
- [12] A. Robert, Y. Liu, M. Nguyen, B. Meunier, Regulation of copper and Iron homeostasis by metal chelators: A possible chemotherapy for alzheimer's disease, *Acc. Chem. Res.* 48 (2015) 1332–1339. <https://doi.org/10.1021/acs.accounts.5b00119>.

- [13] G. Grasso, A.M. Santoro, V. Lanza, D. Sbardella, C. Tundo, Grazia Raffaella Ciaccio, S. Marini, M. Coletta, D. Milardi, The double faced role of copper in A $\beta$  homeostasis: A survey on the interrelationship between metal dyshomeostasis, UPS functioning and autophagy in neurodegeneration, *Coord. Chem. Rev.* 347 (2017) 1–22. <https://doi.org/10.1016/j.ccr.2017.06.004>.
- [14] J. Geng, M. Li, L. Wu, J. Ren, X. Qu, Liberation of copper from amyloid plaques: Making a risk factor useful for alzheimer's disease treatment, *J. Med. Chem.* 55 (2012) 9146–9155. <https://doi.org/10.1021/jm3003813>.
- [15] L.M. Gaetke, H.S. Chow-Johnson, C.K. Chow, Copper: toxicological relevance and mechanisms, *Arch. Toxicol.* 88 (2014) 1929–1938. <https://doi.org/10.1007/s00204-014-1355-y>.
- [16] C. Shen, E.J. New, What has fluorescent sensing told us about copper and brain malfunction?, *Metallomics.* 7 (2015) 56–65. <https://doi.org/10.1039/c4mt00288a>.
- [17] C. Duncan, A.R. White, Copper complexes as therapeutic agents, *Metallomics.* 4 (2012) 127–138. <https://doi.org/10.1039/c2mt00174h>.
- [18] B.M. Paterson, P.S. Donnelly, Copper complexes of bis(thiosemicarbazones): From chemotherapeutics to diagnostic and therapeutic radiopharmaceuticals, *Chem. Soc. Rev.* 40 (2011) 3005–3018. <https://doi.org/10.1039/c0cs00215a>.
- [19] V.S. Zanon, J.A. Lima, T. Cuya, F.R.S. Lima, A.C.C. da Fonseca, J.G. Gomez, R.R. Ribeiro, T.C.C. França, M.D. Vargas, In-vitro evaluation studies of 7-chloro-4-aminoquinoline Schiff bases and their copper complexes as cholinesterase inhibitors, *J. Inorg. Biochem.* 191 (2019) 183–193. <https://doi.org/10.1016/j.jinorgbio.2018.11.019>.
- [20] K. Chand, H.M. Alsoghier, S. Chaves, M.A. Santos, Tacrine-(hydroxybenzoyl-pyridone) hybrids as potential multifunctional anti-Alzheimer's agents: AChE inhibition, antioxidant activity and metal chelating capacity, *J. Inorg. Biochem.* 163 (2016) 266–277. <https://doi.org/10.1016/j.jinorgbio.2016.05.005>.
- [21] L.M.F. Gomes, R.P. Vieira, M.R. Jones, M.C.P. Wang, C. Dyrager, E.M. Souza-Fagundes, J.G. Da Silva, T. Storr, H. Beraldo, 8-Hydroxyquinoline Schiff-base compounds as antioxidants and modulators of copper-mediated A $\beta$  peptide aggregation, *J. Inorg. Biochem.* 139 (2014) 106–116. <https://doi.org/10.1016/j.jinorgbio.2014.04.011>.
- [22] Z. Wang, Y. Wang, W. Li, F. Mao, Y. Sun, L. Huang, X. Li, Design, synthesis, and evaluation of multitarget-directed selenium-containing clioquinol derivatives for the treatment of Alzheimer's disease, *ACS Chem. Neurosci.* 5 (2014) 952–962. <https://doi.org/10.1021/cn500119g>.
- [23] W. Huang, M. Liang, Q. Li, X. Zheng, C. Zhang, Q. Wang, L. Tang, Z. Zhang, B. Wang, Z. Shen,

Development of the “hidden” multifunctional agents for Alzheimer’s disease, *Eur. J. Med. Chem.* 177 (2019) 247–258. <https://doi.org/10.1016/j.ejmech.2019.05.051>.

- [24] M.I. Fernández-Bachiller, C. Pérez, G.C. González-Muñoz, S. Conde, M.G. López, M. Villarroya, A.G. García, M.I. Rodríguez-Franco, Novel tacrine-8-hydroxyquinoline hybrids as multifunctional agents for the treatment of Alzheimer's disease, with neuroprotective, cholinergic, antioxidant, and copper-complexing properties, *J. Med. Chem.* 53 (2010) 4927–4937. <https://doi.org/10.1021/jm100329q>.
- [25] S.R. Bareggi, U. Cornelli, Clioquinol: Review of its mechanisms of action and clinical uses in neurodegenerative Disorders, *CNS Neurosci. Ther.* 18 (2012) 41–46. <https://doi.org/10.1111/j.1755-5949.2010.00231.x>.
- [26] R.A. Cherny, C.S. Atwood, M.E. Xilinas, D.N. Gray, W.D. Jones, C.A. McLean, K.J. Barnham, I. Volitakis, F.W. Fraser, Y.S. Kim, X. Huang, L.E. Goldstein, R.D. Moir, J.T. Lim, K. Beyreuther, H. Zheng, R.E. Tanzi, C.L. Masters, A.I. Bush, Treatment with a copper-zinc chelator markedly and rapidly inhibits  $\beta$ -amyloid accumulation in Alzheimer’s disease transgenic mice, *Neuron*. 30 (2001) 665–676. [https://doi.org/10.1016/S0896-6273\(01\)00317-8](https://doi.org/10.1016/S0896-6273(01)00317-8).
- [27] M.G. Papanikolaou, S. Hadjithoma, D.S. Chatzikypraiou, D. Papaioannou, C. Drouza, A.C. Tsipis, H.N. Miras, A.D. Keramidas, T.A. Kabanos, Investigation of dioxygen activation by copper(II)-iminate/aminato complexes, *Dalt. Trans.* 47 (2018) 16242–16254. <https://doi.org/10.1039/c8dt03137a>.
- [28] J. England, G.J.P. Britovsek, N. Rabadia, A.J.P. White, Ligand topology variations and the importance of ligand field strength in non-heme iron catalyzed oxidations of alkanes, *Inorg. Chem.* 46 (2007) 3752–3767. <https://doi.org/10.1021/ic070062r>.
- [29] G.M. Sheldrick, Phase annealing in SHELX-90: direct methods for larger structures, *Acta Crystallogr. Sect. A.* 46 (1990) 467–473. <https://doi.org/10.1107/S0108767390000277>.
- [30] G.M. Sheldrick, A short history of SHELX, *Acta Crystallogr. Sect. A Found. Crystallogr.* 64 (2008) 112–122. <https://doi.org/10.1107/S0108767307043930>.
- [31] L.J. Farrugia, WinGX suite for small-molecule single-crystal crystallography, *J. Appl. Crystallogr.* 32 (1999) 837–838. <https://doi.org/10.1107/S0021889899006020>.
- [32] R.C. Clark, J.S. Reid, The analytical calculation of absorption in multifaceted crystals, *Acta Crystallogr. Sect. A.* 51 (1995) 887–897. <https://doi.org/10.1107/S0108767395007367>.
- [33] A.T. Welzel, J.E. Maggio, G.M. Shankar, D.E. Walker, B.L. Ostaszewski, S. Li, I. Klyubin, M.J. Rowan, P. Seubert, D.M. Walsh, D.J. Selkoe, Secreted amyloid  $\beta$ -proteins in a cell culture model include N-terminally extended peptides that impair synaptic plasticity, *Biochemistry.* 53 (2014) 3908–

3921. <https://doi.org/10.1021/bi5003053>.

- [34] A.W. Addison, T.N. Rao, J. Reedijk, J. van Rijn, G.C. Verschoor, Synthesis, Structure, and Spectroscopic Properties of Copper(II) Compounds containing Nitrogen-Sulphur Donor Ligands ; the Crystal and Molecular Structure of Aqua[1,7-bis(N-methylbenzimidazol-2'-yl)-2,6-dithiaheptane]copper(II) Perchlorate, *J. CHEM. SOC. Dalt. TRANS.* (1984) 1349–1356. <https://doi.org/https://doi.org/10.1039/DT9840001349>.
- [35] S.L. Jain, P. Bhattacharyya, H.L. Milton, A.M.Z. Slawin, J.A. Crayston, J.D. Woollins, New pyridine carboxamide ligands and their complexation to copper (II). X-Ray crystal structures of mono-, di, tri- and tetranuclear copper complexes, *Dalt. Trans.* (2004) 862–871. <https://doi.org/https://doi.org/10.1039/B316519A>.
- [36] J. Wang, B. Djukic, J. Cao, A. Alberola, F.S. Razavi, M. Pilkington, A novel bis tridentate bipyridine carboxamide ligand and its complexation to copper(II): Synthesis, structure, and magnetism, *Inorg. Chem.* 46 (2007) 8560–8568. <https://doi.org/10.1021/ic700469v>.
- [37] N.J. Hurley, J.J. Hayward, J.M. Rawson, M. Murrie, M. Pilkington, Exploring the coordination chemistry of 3,3'-Di(picolinamoyl)-2,2'- bipyridine: One ligand, multiple nuclearities, *Inorg. Chem.* 53 (2014) 8610–8623. <https://doi.org/10.1021/ic501224q>.
- [38] K. Majee, J. Patel, B. Das, S.K. Padhi,  $\mu$ -Pyridine-bridged copper complex with robust proton-reducing ability, *Dalt. Trans.* 46 (2017) 14869–14879. <https://doi.org/10.1039/c7dt03153j>.
- [39] S.S. Harmalkar, R.J. Butcher, V. V. Gobre, S.K. Gaonkar, L.R. D'Souza, M. Sankaralingam, I. Furtado, S.N. Dhuri, Synthesis, characterization and antimicrobial properties of mononuclear copper(II) compounds of N,N'-di(quinolin-8-yl)cyclohexane-1,2-diamine, *Inorganica Chim. Acta.* 498 (2019) 119020. <https://doi.org/10.1016/j.ica.2019.119020>.
- [40] V. Oliveri, G.I. Grasso, F. Bellia, F. Attanasio, M. Viale, G. Vecchio, Soluble sugar-based quinoline derivatives as new antioxidant modulators of metal-induced amyloid aggregation, *Inorg. Chem.* 54 (2015) 2591–2602. <https://doi.org/10.1021/ic502713f>.
- [41] Y. Ji, H.J. Lee, M. Kim, G. Nam, S.J.C. Lee, J. Cho, C.M. Park, M.H. Lim, Strategic Design of 2,2'-Bipyridine Derivatives to Modulate Metal-Amyloid- $\beta$  Aggregation, *Inorg. Chem.* 56 (2017) 6695–6705. <https://doi.org/10.1021/acs.inorgchem.7b00782>.
- [42] M.B. Podlisny, B.L. Ostaszewski, S.L. Squazzo, E.H. Koo, R.E. Rydell, D.B. Teplow, D.J. Selkoe, Aggregation of secreted amyloid  $\beta$ -protein into sodium dodecyl sulfate-stable oligomers in cell culture, *J. Biol. Chem.* 270 (1995) 9564–9570. <https://doi.org/10.1074/jbc.270.16.9564>.
- [43] K. Nieweg, A. Andreyeva, B. Van Stegen, G. Tanriöver, K. Gottmann, Alzheimer's disease-related

- amyloid- $\beta$  induces synaptotoxicity in human iPS cell-derived neurons, *Cell Death Dis.* 6 (2015) 1–13. <https://doi.org/10.1038/cddis.2015.72>.
- [44] J. Kovalevich, D. Langford, Considerations for the Use of SH-SY5Y Neuroblastoma Cells in Neurobiology, *Methods Mol. Biol.* 1078 (2013) 9–21. [https://doi.org/10.1007/978-1-62703-640-5\\_2](https://doi.org/10.1007/978-1-62703-640-5_2).
- [45] M. Encinas, M. Iglesias, Y. Liu, H. Wang, A. Muhaisen, V. Ceña, C. Gallego, J.X. Comella, Sequential treatment of SH-SY5Y cells with retinoic acid and brain-derived neurotrophic factor gives rise to fully differentiated, neurotrophic factor-dependent, human neuron-like cells, *J. Neurochem.* 75 (2000) 991–1003. <https://doi.org/10.1046/j.1471-4159.2000.0750991.x>.
- [46] M.M. Shipley, C.A. Mangold, M.L. Szpara, Differentiation of the SH-SY5Y human neuroblastoma cell line, *J. Vis. Exp.* 2016 (2016) 1–11. <https://doi.org/10.3791/53193>.
- [47] L. Agholme, T. Lindström, K. Kagedal, J. Marcusson, M. Hallbeck, An in vitro model for neuroscience: Differentiation of SH-SY5Y cells into cells with morphological and biochemical characteristics of mature neurons, *J. Alzheimer's Dis.* 20 (2010) 1069–1082. <https://doi.org/10.3233/JAD-2010-091363>.
- [48] H. Shaykhalishahi, R. Yazdanparast, H.H. Ha, Y.T. Chang, Inhibition of H<sub>2</sub>O<sub>2</sub>-induced neuroblastoma cell cytotoxicity by a triazine derivative, AA3E2, *Eur. J. Pharmacol.* 622 (2009) 1–6. <https://doi.org/10.1016/j.ejphar.2009.07.017>.
- [49] C.S. Jiang, Y. Fu, L. Zhang, J.X. Gong, Z.Z. Wang, W. Xiao, H.Y. Zhang, Y.W. Guo, Synthesis and biological evaluation of novel marine-derived indole-based 1,2,4-oxadiazoles derivatives as multifunctional neuroprotective agents, *Bioorganic Med. Chem. Lett.* 25 (2015) 216–220. <https://doi.org/10.1016/j.bmcl.2014.11.068>.
- [50] Y. Chen, B. Wu, Y. Hao, Y. Liu, Z. Zhang, C. Tian, X. Ning, Y. Guo, J. Liu, X. Wang, Structure-activity relationship studies of (E)-3,4-dihydroxystyryl alkyl sulfones as novel neuroprotective agents based on improved antioxidant, anti-inflammatory activities and BBB permeability, *Eur. J. Med. Chem.* 171 (2019) 420–433. <https://doi.org/10.1016/j.ejmech.2019.03.044>.
- [51] G. Wendt, V. Kemmel, C. Patte-Mensah, B. Uring-Lambert, A. Eckert, M.J. Schmitt, A.G. Mensah-Nyagan, Gamma-hydroxybutyrate, acting through an anti-apoptotic mechanism, protects native and amyloid-precursor-protein-transfected neuroblastoma cells against oxidative stress-induced death, *Neuroscience.* 263 (2014) 203–215. <https://doi.org/10.1016/j.neuroscience.2013.12.067>.
- [52] N.C. Inestrosa, A. Alvarez, C.A. Pérez, R.D. Moreno, M. Vicente, C. Linker, O.I. Casanueva, C. Soto, J. Garrido, Acetylcholinesterase accelerates assembly of amyloid- $\beta$ -peptides into Alzheimer's fibrils: Possible role of the peripheral site of the enzyme, *Neuron.* 16 (1996) 881–891.

[https://doi.org/10.1016/S0896-6273\(00\)80108-7](https://doi.org/10.1016/S0896-6273(00)80108-7).

- [53] A. Alvarez, C. Opazo, R. Alarcón, J. Garrido, N.C. Inestrosa, Acetylcholinesterase promotes the aggregation of amyloid- $\beta$ -peptide fragments by forming a complex with the growing fibrils, *J. Mol. Biol.* 272 (1997) 348–361. <https://doi.org/10.1006/jmbi.1997.1245>.
- [54] R. Cai, L.N. Wang, J.J. Fan, S.Q. Geng, Y.M. Liu, New 4-N-phenylaminoquinoline derivatives as antioxidant, metal chelating and cholinesterase inhibitors for Alzheimer's disease, *Bioorg. Chem.* 93 (2019) 103328. <https://doi.org/10.1016/j.bioorg.2019.103328>.
- [55] A. Garcimartín, M.E. López-Oliva, M.P. González, F.J. Sánchez-Muniz, J. Benedí, Hydrogen peroxide modifies both activity and isoforms of acetylcholinesterase in human neuroblastoma SH-SY5Y cells, *Redox Biol.* 12 (2017) 719–726. <https://doi.org/10.1016/j.redox.2017.04.004>.
- [56] E.M. Molochkina, O.M. Zorina, L.D. Fatkullina, A.N. Goloschapov, E.B. Burlakova, (30)  $H_2O_2$  modifies membrane structure and activity of acetylcholinesterase, *Chem. Biol. Interact.* 157–158 (2005) 401–404. <https://doi.org/10.1016/j.cbi.2005.10.075>.
- [57] D. Yao, J. Wang, G. Wang, Y. Jiang, L. Shang, Y. Zhao, J. Huang, S. Yang, J. Wang, Y. Yu, Design, synthesis and biological evaluation of coumarin derivatives as novel acetylcholinesterase inhibitors that attenuate  $H_2O_2$ -induced apoptosis in SH-SY5Y cells, *Bioorg. Chem.* 68 (2016) 112–123. <https://doi.org/10.1016/j.bioorg.2016.07.013>.
- [58] M.I. Rocha, M.J. Rodrigues, C. Pereira, H. Pereira, M.M. da Silva, N.R. da Neng, J.M.F. Nogueira, J. Varela, L. Barreira, L. Custódio, Biochemical profile and in vitro neuroprotective properties of *Carpobrotus edulis* L., a medicinal and edible halophyte native to the coast of South Africa, *South African J. Bot.* 111 (2017) 222–231. <https://doi.org/10.1016/j.sajb.2017.03.036>.
- [59] P. Bar-On, C.B. Millard, M. Harel, H. Dvir, A. Enz, J.L. Sussman, I. Silman, Kinetic and structural studies on the interaction of cholinesterases with the anti-Alzheimer drug rivastigmine, *Biochemistry.* 41 (2002) 3555–3564. <https://doi.org/10.1021/bi020016x>.
- [60] O. Trott, A.J. Olson, AutoDock Vina: improving the speed and accuracy of docking with a new scoring function, efficient optimization and multithreading, *J. Comput. Chem.* 31 (2010) 455–461. <https://doi.org/10.1002/jcc.21334>.

**Supplementary Material**

**Supplementary Table 1**

**Supplementary Figure 1**

**Table S1**

Docking studies and affinities for the interaction of AChE with the synthesized metal chelators.

Energies of all poses of H <sub>2</sub> dqpyca		dist from best mode	
Mode	affinity <sup>a</sup> (kcal/mol)	rmsd <sup>b</sup> l.b.	rmsd u.b.
1	-13.6	0.000	0.000
2	-13.5	0.576	9.455
3	-12.8	1.476	9.748
4	-12.6	2.410	9.994
5	-12.5	2.081	9.986
6	-12.5	1.974	10.001
7	-12.5	1.957	3.200
8	-12.4	2.192	9.804
9	-12.4	2.184	3.433

Energies of all poses of Hbpq		dist from best mode	
Mode	affinity (kcal/mol)	rmsd l.b.	rmsd u.b.
1	-9.8	0.000	0.000
2	-9.6	2.630	6.389
3	-9.3	1.570	2.031
4	-9.2	4.348	6.138
5	-8.9	2.701	3.456
6	-8.9	4.426	6.000
7	-8.9	4.401	5.554
8	-8.9	2.409	3.714
9	-8.7	5.612	7.752

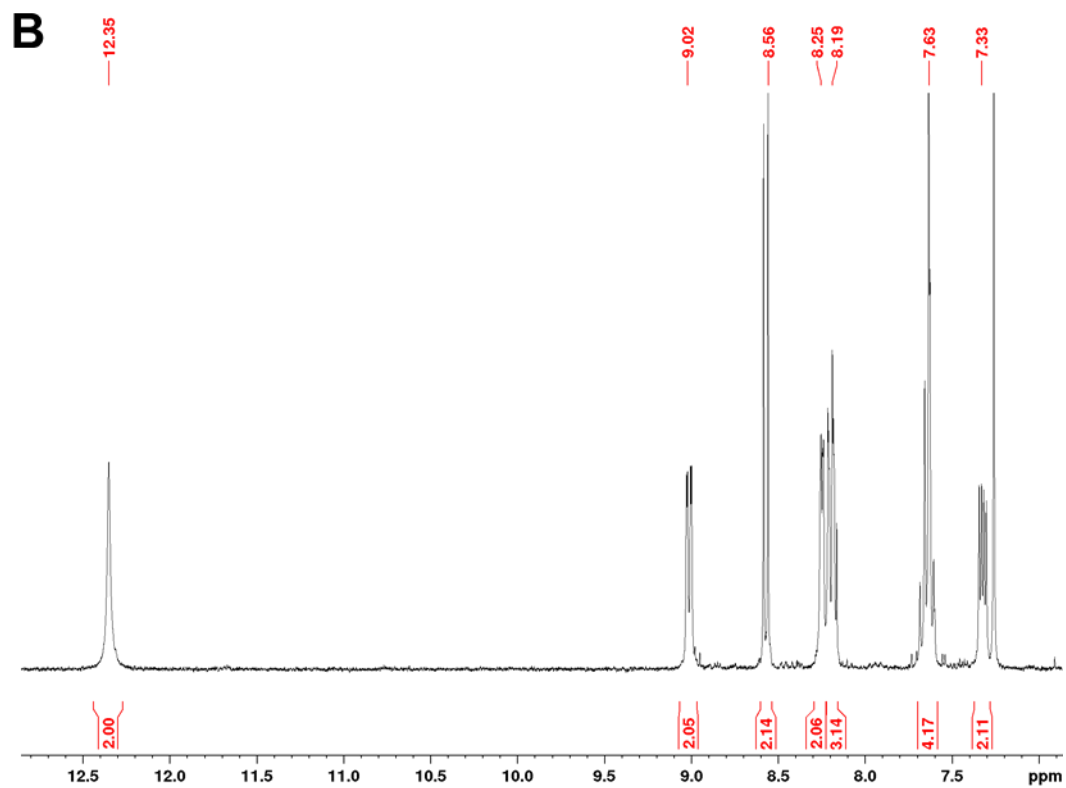
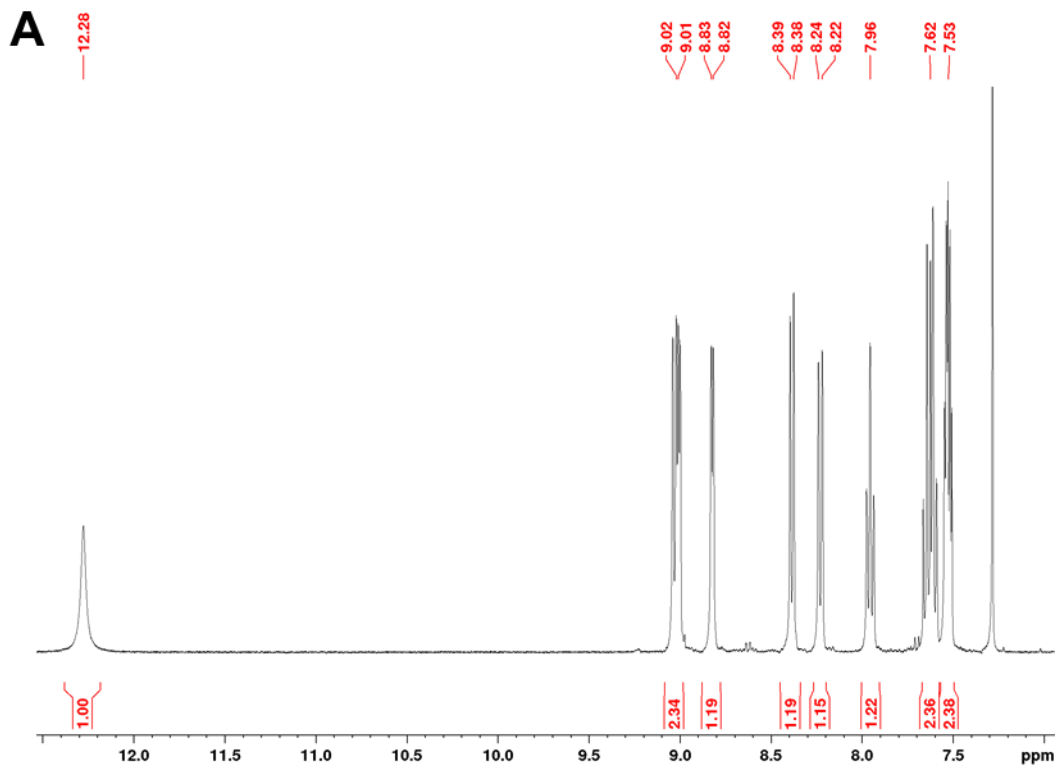
  

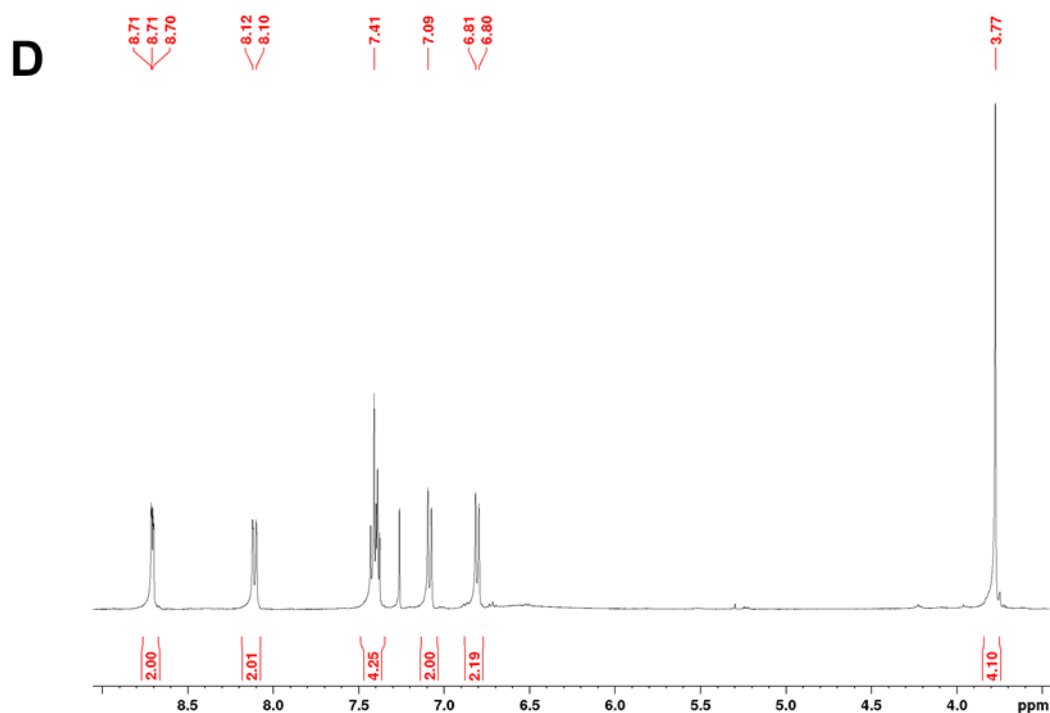
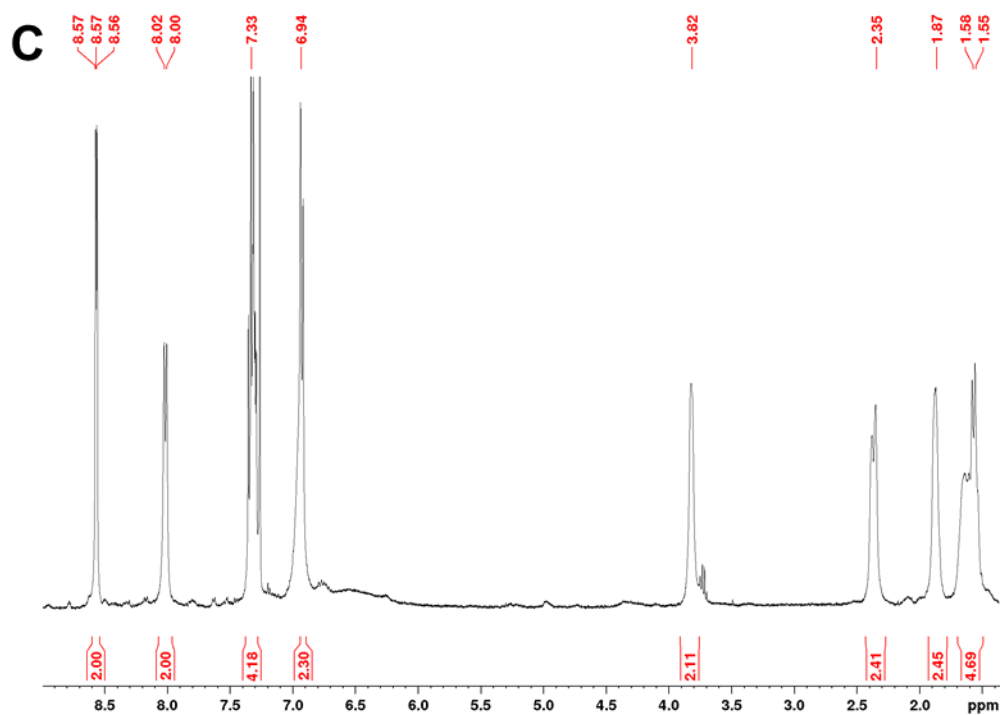
Energies of all poses of H <sub>2</sub> bqch		dist from best mode	
Mode	affinity (kcal/mol)	rmsd l.b.	rmsd u.b.
1	-12.7	0.000	0.000
2	-12.3	0.204	7.045
3	-12.1	1.632	2.275
4	-11.9	1.623	6.444
5	-10.8	1.748	5.797
6	-10.7	3.460	5.907
7	-10.6	2.258	8.730
8	-10.3	4.637	9.797
9	-10.3	4.611	7.911

Energies of all poses of H <sub>2</sub> bqen		dist from best mode	
Mode	affinity (kcal/mol)	rmsd l.b.	rmsd u.b.
1	-11.3	0.000	0.000
2	-11.3	0.084	7.659
3	-10.9	2.034	3.616
4	-10.6	1.969	5.801
5	-10.5	1.075	1.383
6	-10.1	3.345	8.807
7	-10.0	3.385	8.409
8	-9.9	1.102	2.013
9	-9.9	3.386	4.839

<sup>a</sup> Affinity describes the energy of the pose and is related to the stability of the interaction of AChE with the synthesized metal chelators. The more negative this value is, the more stable the interaction. <sup>b</sup> Rmsd values indicate how close the extra poses of the tested quinoline-based metal chelator is to that of the best mode.





**Fig. S1.**  $^1\text{H}$  NMR spectra of the synthesized ligands. (A)  $^1\text{H}$  NMR spectrum of **Hbpq** in  $\text{CDCl}_3$ . (B)  $^1\text{H}$  NMR spectrum of **H2dqpyca** in  $\text{CDCl}_3$ . (C)  $^1\text{H}$  NMR spectrum of **H2bqch** in  $\text{CDCl}_3$ . (D)  $^1\text{H}$  NMR spectrum of **H2bqen** in  $\text{CDCl}_3$ .